Chapter 1
3D-Printed Soft Wearable Electronics: Techniques, Materials, and Applications

Yuxuan Liu and Yong Zhu

1.1 Background

Wearable electronics with soft features are emerging in recent years, enabling long-term applications on the human body. For example, wearable sensors can provide accurate monitoring of human physiological signals; [1–6] wearable drug delivery systems and wearable heaters can ensure precise and timely therapy; [7–10] and wearable displays with the visual interface can clearly inform the monitoring status [11]. Not only for human health, wearable devices can also be used on plants to monitor plant health for smart agriculture [12, 13]. Wearable electronics that feature gas permeability [14] and recyclability [15] have emerged, which further facilitate practical application of these wearable devices. Relatively simple and cost-effective fabrication of soft wearable electronics can greatly facilitate their deployment. Top-down microfabrication, e.g., deposition/evaporation, lithography, and etching, are conventional approaches for device fabrication [16–20]. They are widely used in the fabrication of electronics with high resolution and high integration levels [21–24]. However, they are typically complicated and expensive. Instead of top-down approaches, bottom-up approaches including coating and printing techniques are widely used to process nanomaterials with high throughput and low costs [25–28]. However, coating techniques and conventional printing techniques (e.g., inkjet printing, screen printing, and gravure printing) are typically limited to 2D planar fabrication; hence, most of the devices, including wearable soft sensors, actuators,

Y. Liu · Y. Zhu (✉)
Department of Mechanical and Aerospace Engineering, North Carolina State University, Raleigh, NC 27695, USA
e-mail: yong_zhu@ncsu.edu

Y. Liu
e-mail: yliu235@ncsu.edu

K. Zhou (ed.), *Additive Manufacturing*,
https://doi.org/10.1007/978-3-031-04721-3_1

and transistors, are relatively simple in architecture. To adapt to complex wearable electronics systems, 3D printing technique has been used to fabricate 3D structured devices. There are generally two approaches to constructing 3D structures by printing: (1) directly 3D printing functional materials or functional/structural composite materials onto a planar substrate and (2) printing 2D traces or 3D structures on a preformed 3D structure to enable the function.

Applying 3D printing to the fabrication of soft wearable electronics can offer the following advantages: (1) enabling rapid prototyping due to the simple setup and continuous fabrication process; (2) providing low-cost and large-scale fabrication for industrial applications; [3] being compatible with printing of multi-materials to reduce the time and cost; and [4] making flexible hybrid electronics including multi-materials and multi-structures possible. In this chapter, soft wearable electronics fully or partially fabricated by 3D printing techniques will be introduced. Wearable electronics are typically composited of several parts: a soft substrate for wearability, functional materials-enabled electrical components, and highly conductive interconnects.

1.2 3D Printing Techniques Used in Soft Wearable Electronics

1.2.1 Photopolymerization-Based Printing Approaches

Photopolymerization is among the mechanisms of the first-generation 3D printing techniques. Typically, ultraviolet (UV) light is used to solidify the photo-hardening polymer resin locally to pattern the structure layer-by-layer until a final 3D object is accomplished. The exposure of light over the material generates the desired pattern according to the G-code or CAD model. Photopolymerization-based 3D printing techniques, including stereo lithography appearance (SLA), digital light processing (DLP), and continuous direct light processing (CDLP) are representative approaches using the photopolymerization mechanism to construct 3D polymer structures. Materials that can be printed using photopolymerization-based printing approaches are usually photosensitive polymer resins that can be solidified by radiation (e.g., UV or visible light) [29]. The chemical, optical, and rheological properties need to be carefully considered when choosing proper materials for printing. Photosensitive polymers with functional groups such as acrylates, epoxides, thiolenes, and fumarates are commonly used. Acrylate oligomer, UV curable polydimethylsiloxane (PDMS), UV curable polyurethane acrylate, and commercially available photopolymer Tango-Plus FLX930 have been 3D-printed as soft substrates or structural materials for soft electronics [30–33].

SLA and DLP are two most widely used photopolymerization-based printing approaches. In the conventional SLA process, a laser source across the polymer surface is utilized for performing the direct laser writing locally, as shown in Fig. 1.1a.

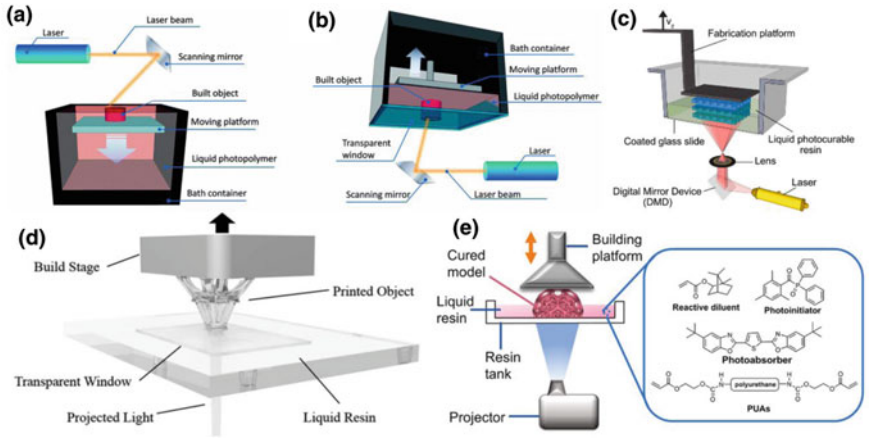

Fig. 1.1 Schematic representations of **a** conventional SLA printing [35], **b** modified SLA printing [35] and **c** DLP printing system [36]. **d** A fast fabrication method of high-resolution features using SLA printing [34]. **e** A DLP printer for the fabrication of a high-resolution 3D solid object and the composition of a photocurable resin [37]

Recently, the projection type SLA printers are developed, where the pattern is formed when the UV light goes through a transparent window and solidifies the resin layer-by-layer, as shown in Fig. 1.1b. In the DLP process, a digital mirror device is used to project the UV light on a whole layer to solidify the design pattern in one shot, as shown in Fig. 1.1c. Attributed to the capability of printing polymer materials, these methods have been used to fabricate the substrate or structural frameworks for wearable electronics in recent years. Zarek et al. demonstrated the fabrication of complex shape memory structures with a viscous melt (≈30 Pa s) using a commercial SLA printer (Picoplus39, Asiga) and a customized heated resin bath. The printing setup is shown in Fig. 1.1c. For each layer, the light source projects a cross-section of the part on a thin layer of resin in contact with the print platform. The platform then exits the photopolymer resin and restarts the process for another layer. Odent et al. used an Ember (Autodesk, Inc.) digital mask projection SLA printer to fabricate ionic conductors with high stretchability (up to 425%) and high toughness (up to 53.5 kJ m^{-3}) [34]. The printer employs a bottom-up process, where the photo-pattern is projected through a transparent, oxygen permeable window at the base of a vat of liquid resin (Fig. 1.1d). Peng et al. printed 3D polyurethane acrylate oligomer (PUA) elastomers structures by a homemade DLP 3D printer, as shown in Fig. 1.1e. Because the DLP printers share a similar mechanism with the video projector, a commercial video projector (1920 × 1080 pixels) with 405 nm UV light was used as the light source and the digital mirror device. The printed elastomer was then combined with the stretchable and conductive hydrogels to fabricate a piezoresistive strain sensor and a wearable finger motion monitoring sensor.

Advantages and drawbacks exist when these techniques are used in fabricating wearable electronics. SLA is capable of printing large-size models and the technique

is mature. However, the resolution is limited by the size of the laser beam, and the printing speed is relatively slow in the conventional SLA system. It was reported that it took 44 min to print a 1 cm^3 cube with a 100 μm layer thickness using an SLA printer [38]. DLP has the greatest advantage of high resolution, however, structures need to be small in size to achieve the high precision.

1.2.2 Extrusion-Based Printing Approaches

In the extrusion-based 3D printing, a computer-controlled nozzle directly deposits the material onto the substrate. Typically, pneumatic actuation systems are used for the extrusion of ink through the nozzle. Fused Deposition Modeling (FDM) is the most common 3D printing technique due to the advantages of easy implementation, simplicity, and low costs. In an FDM printing process, the thermoplastic materials are molten in the heated nozzle and deposited on the substrate in a layer-by-layer manner to obtain the desired 3D shape, as shown in Fig. 1.2a. FDM technique has been widely used to fabricate the substrate or structural framework for wearable electronics [39–41]. Liang et al. developed an FDM method to fabricate a mouthguard type wearable oral delivery device, which can deliver a preloaded compound in the oral cavity to treat local oral disease [41]. Poly(L-lactic acid) (PLA) and poly(vinyl alcohol)

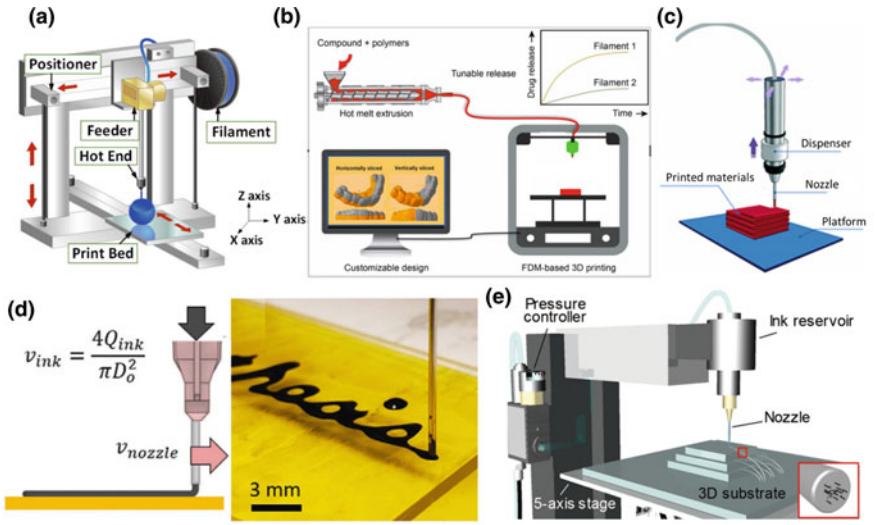

Fig. 1.2 **a** Schematic representation of the FDM printing system [42]. **b** Manufacture process of wearable oral delivery mouthguards using FDM 3D printing [41] **c** Schematic representation of the DIW printing system [35]. **d** Printed letters using CNT ink by the DIW printing technique [43]. **e** Schematic illustration of the DIW system for printing liquid metal/carbon nanotube composites [44]

(PVA) are used as thermoplastic printing materials to construct the device due to their nontoxicity and biocompatibility. The schematic setup is shown in Fig. 1.2b. The manufacture of the oral delivery mouthguards by FDM involved two stages. First, the maxillary anatomy of the subject was scanned and used as the template for 3D printing. Second, the structural materials, PLA and PVA loaded with drugs are hot-melted and extruded into the customizable designed 3D structure based on the scanned template.

Direct ink writing (DIW) is another popular method for 3D printing of both the substrate materials and the functional materials for wearable electronics (Fig. 1.2c) [45–47]. The process of the DIW printing starts with precisely controlling the position of the nozzle following a 3D model and hence the extrusion of fluidic inks to print the designed structures. Unlike the FDM printing, DIW printing does not need a hot nozzle to melt the printing materials for extrusion but requires the ink to be a liquid phase with shear-thinning rheology property and suitable viscosity. Non-Newtonian fluids whose viscosity is a function of the shear rate are the most widely used types of ink for DIW printing. The viscosity of the inks ranges from 10^5 (under a low shear rate of 10^{-2} s^{-1}) to 10^1 Pa s (under a high shear rate of to 10^2 s^{-1}) [46, 48]. Typically, after the inks are extruded and settled down on the substrate, the solidification is achieved by the evaporation of solvents in the ink naturally in the air or by post treatment. Owens et al. used an aqueous carbon nanotube (CNT)-based ink in DIW to fabricate conductive and flexible conductors on polymer and paper substrates [43]. However, the patterns are mostly 2D structures although they used a 3D printer for the fabrication (Fig. 1.2d). Park et al. used a 3D printer for direct writing of liquid metal/CNT composite ink [44]. The printing system and the printed structures are shown in Fig. 1.2e. Benefitting from the oxidation layer outside the liquid metal after printing, the printed structure could be self-standing with a high aspect ratio to maintain a 3D form. The printed 3D traces are demonstrated to be potentially used as interconnects for electronics.

Extrusion-based printing techniques have unique advantages compared to other 3D printing methods. They are more precise in controlling the deposition of materials into 3D structures. The substrates can be versatile. Furthermore, specific techniques such as DIW are compatible with emerging functional materials such as nanomaterials. However, the hot-melting-based FDM methods require thermoplastic polymers as the printing materials; the DIW based methods require the ink to have unique rheological properties, but a clear link between the rheological properties of inks and the device performance is not established. To apply these printing methods, the printing materials and the ink properties need to be tuned carefully to meet the required thermal melting properties, viscosity, and rheological properties.

1.2.3 Powder Bed-Based Printing Approaches

Powder bed-based 3D printing uses powder materials as the feeding materials during the printing. After sintering or binding the designed structure on one layer, another

layer of powder will be fed, and the patterning of this layer continues. Typical powder bed-based 3D printing approaches include binder jetting and selective laser sintering (SLS). Based on the design from a digital file, binder jetting uses binder materials to solidify the designed structure and SLS uses laser to fuse the powder into the designed pattern. SLS has been used to fabricate components for wearable electronics, due to its capabilities to print both metal-based materials and polymers. The powders used for the SLS process should be able to absorb energy at the laser wavelength efficiently [29]. When choosing the printed materials, a suitable laser with the corresponding wavelength should be used. Zacharatos et al. studied the printing performance of silver nanoparticles (AgNPs) using SLS (wavelength of the laser: 532 nm) with high printing speed and high repetition rate (the number of pulses that occur per unit time at a particular point), as shown in Fig. 1.3a [49]. High-quality laser sintering of AgNP patterns with sub 100 μm width (Fig. 1.3b) were achieved with the scanning speed as high as 1 m/s and resistivity down to 8.91 ± 0.9 μ Ω cm. By tuning the laser pulse width and power, different printing performances such as resistivity of the printed NPs can be tailored. Considering that AgNPs are one of the most widely used conductive materials in soft wearable devices, this approach is promising for fabricating fine conducting paths for wearable electronics.

Considering that the feeding materials are in powders, SLS also shows great capability to print 3D structured polymer/conducting filler composites, in which the feeding materials are polymer powders with conducing materials wrapping these powders [49–52]. Li et al. have developed a process to construct a 3D electrically conductive network in a polymer matrix by SLS, as shown in Fig. 1.3c. The feeding powder was CNT-wrapped thermoplastic polyurethane (TPU) powder. Electrical conductivity of the printed TPU/CNT composite reached 10^{-1} S m^{-1}, which is seven orders of magnitude higher than that of the injected one. The cyclic stretching test of the printed TPU/CNT composite showed a 40% increase after 1000 stretching cycles, while no considerable change was observed after 1000 bending cycles. The same group also printed PDMS/CNT composites using SLS [50]. Covalent adaptable PDMS network with dynamic steric-hindrance pyrazole urea bond was first developed and fabricated into powders wrapped by CNTs, as shown in Fig. 1.3c. Furthermore, the printed PDMS/CNT composite possesses self-healing capability due to the presence of the dynamic reversible bonds.

When applying SLS printing to fabricate components for wearable devices, one of the typical issues that needs to be addressed is that the printing materials need to be manufactured into the powder phase in order to be compatible with conventional SLS printing systems, which makes it difficult to print liquid- or solvent-based materials such as liquid metal and nanomaterials suspended in solvents. To address this issue, a modified SLS was developed to combine the sintering process with an inkjet printing system so that liquid phased inks can be printed by the SLS techniques [53].

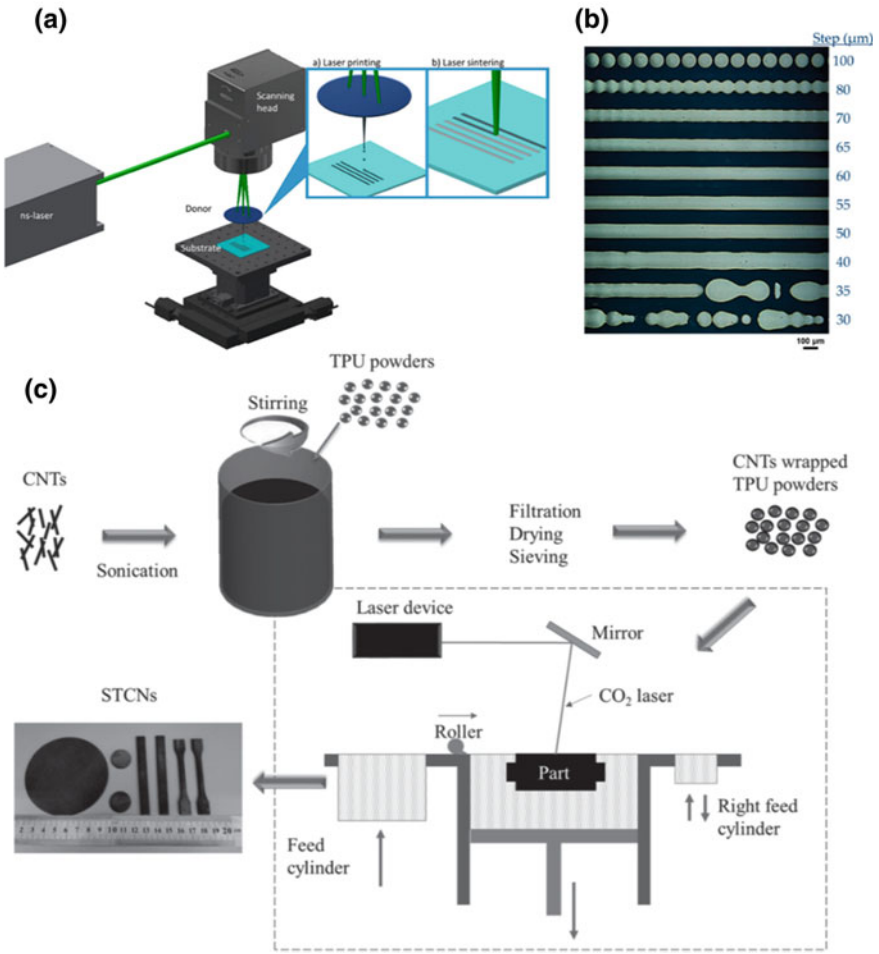

Fig. 1.3 **a** High speed laser printing and laser sintering set-up schematic representation [49]. **b** Microscope images of SLS printed AgNPs. **c** Schematic illustration of the procedures of preparing TPU/CNTs composites by SLS [50]

1.3 3D Printable Materials for Soft Wearable Electronics

Using traditional materials for soft wearable electronics is challenging due to the fact that most metallic and semiconducting materials are lack of flexibility and conformability [54, 55]. However, large strain (up to 100%) needs to be accommodated when being worn on the human body due to the daily motion of humans. To make the 3D-printed electronics deformable for wearable applications, both the printed materials and the structure design are crucial. The biocompatibility of these materials is also of great importance for the practical application of wearable electronics. Some

excellent reviews have been devoted to the biocompatibility of wearable devices [56–63]. Hence this section will not discuss the details about the biocompatibility of 3D-printed materials for wearable electronics. In this section, the 3D printable materials and the associated 3D printing systems for printing these materials will be discussed. First, the mechanics consideration of the printed structures is briefly introduced. Then, widely used materials for building blocks of soft wearable electronics are summarized, including featured 3D printing systems. These 3D printable materials include functional materials such as conductive materials, dielectric materials and structural materials such as elastomers and shape memory polymers. In this section, metal-based materials and carbon-based materials are discussed due to their wide applications in soft wearable electronics. Metal-based materials include nanostructured metal materials and molten/liquid metal, while typical carbon materials include CNTs and graphene. Polymer materials include conductive polymer, shape memory polymer, and polymer for soft substrates.

1.3.1 Mechanics Consideration

There are two typical ways to achieve the stretchability of a device. One way is to print intrinsically stretchable materials such as polymers and composites containing nanomaterials. The other is to print stretchable architectures such as serpentine structure [64], wavy structure [47], web/mesh structure [65, 66], origami/kirigami structure [67], scaffold/matrix structure [37, 68–70] and helix/spiral structure [64, 71, 72]. The 3D-printed materials can either be self-standing or on a stretchable substrate. Often these two strategies are combined to improve stretchability/compressibility. Wang et al. developed a fully 3D-printed sensor using elastomer as the substrate, TPU/Ag nanoflakes composite as the electrode, and TPU/porous carbon black as the piezoresistive sensor [73]. The electrodes are printed into a helix structure to reduce the strain interference, as shown in Fig. 1.4a. The electrode layer with an 85% Ag content can be stretched up to 120% without losing conductivity; the resistance changes only 7% when the electrode is stretched by 50% strain, attributed to the inherent stretchability of TPU and the helix structure. Wong et al. developed a 3D printable shear-thinning ionogel with ionic conductivity [74]. By printing the ionogel into auxetic geometry (as shown in Fig. 1.4b), the fabricated sensor exhibits 310% higher stretchability compared to a continuous bulk film. The extremely high stretchability is due to the auxetic structure that exhibits in-plane and out-of-plane deformation to reduce the local stress during tensile stretching. Wei et al. printed 3D wavy structured conductors using PDMS/CNT composite ink [47]. The authors studied the effect of joining angles (θ) on the stretchability of the wavy conductor (shown in Fig. 1.4c, d), and found that a 45° joining angle results in the best mechanical stretchability. With the help of the wavy structure, the 3D-printed wavy structure can be stretched up to 315%; the resistance change is only 5% when stretched by 100% strain. These structural design strategies for improving the stretchability of the printed materials present a great opportunity for 3D printing due to its facile manufacturing process for these

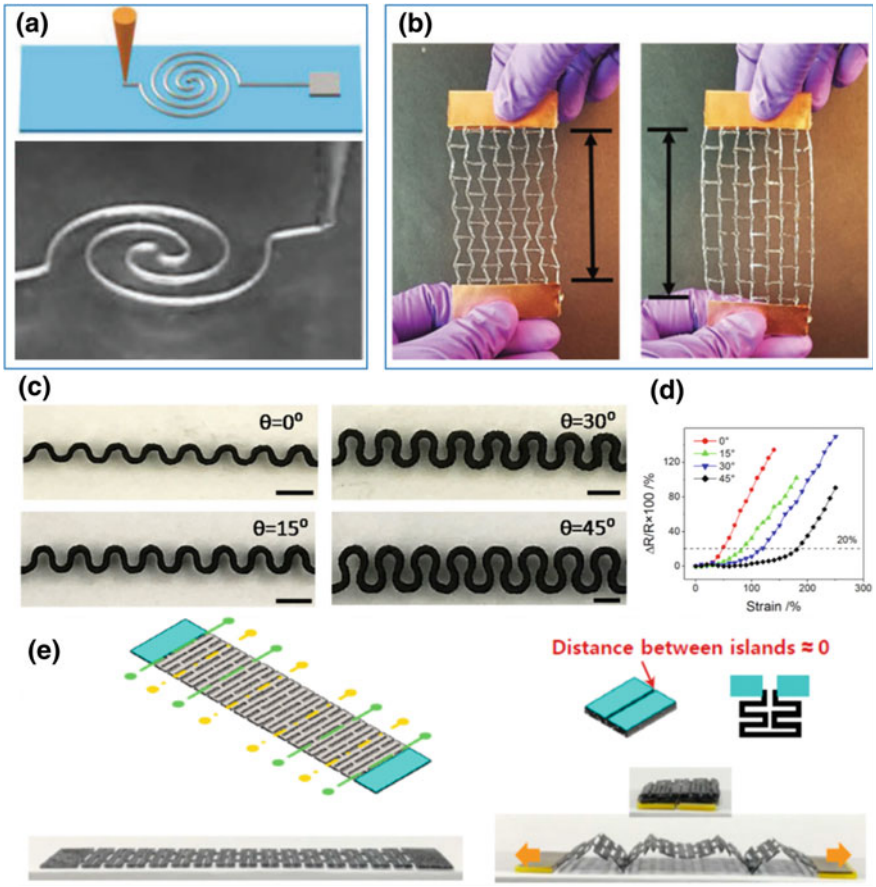

Fig. 1.4 **a** Helix structured TPU/Ag nanoflake electrode [73]. **b** The printed and crosslinked auxetic structure expands in the direction perpendicularly to the loading direction [74]. **c** The cross-sectional images of the 3D-printed wavy electrodes with different joining angles. Scale bar 5 mm [47]. **d** Relative resistance change versus applied strain on the electrodes with different joining angles [47]. The illustration of combining kirigami and origami design for minimizing the device size and enhancing the stretchability [67]

complex structures, which may not be applicable to other fabrication approaches. Jo et al. demonstrated a 3D printing-assisted approach to print TPU structures on a AgNW network film by FDM printing to fabricate AgNWs/TPU composite structures [67]. The printed structure can be used as stretchable conductor. To further enhance the stretchability, kirigami and origami structures were employed, which provides high stretchability and efficient space utilization, as shown in Fig. 1.4e.

1.3.2 Metal-Based Materials

Metal-based materials possess the advantages of high conductivity, which is critical for electronics. Conductors are one of the most important building blocks in electronic systems to act as electrodes, interconnects, and sensing parts. Higher conductivity leads to more efficient signal transmission and lower power consumption, which are the key to the performance of electronic systems. However, manufacturing of metal-based materials for wearable electronics needs further improvement to meet the requirement of low costs, scalability, and capability of patterning complex structures. Additive manufacturing approaches such as 3D printing are promising to fabricate and pattern metal-based materials. In this section, 3D printing of metal-based materials used in soft wearable electronics including nanostructures and low melting-point metals is summarized. Their printing features and performance will be discussed.

1.3.2.1 Nanostructures (Nanoparticles, Nanowires, and Nanoflakes)

Development of advanced materials especially nanomaterials has provided unprecedented mechanical, electrical, optical and other properties to wearable electronics [5, 75–79]. Furthermore, advanced facile and low-cost 3D printing techniques enable the large-scale manufacturing of these materials, which is critical for next-generation wearable consumer electronics. Conductive nanomaterial composites, with either insulating or conductive polymer matrices, are amongst the most promising candidates for the electrodes of wearable sensors [5, 14, 76, 78, 80]. Metal NPs are the most widely used conductive building block for electrodes, interconnects, and sensing components in wearable electronics. By mixing the NPs into a polymer matrix, moderate electrical conductivity and mechanical stretchability can be achieved attributed to the percolation structure of NP conductive traces. With proper mechanical design for the printed structure, the electrical and mechanical properties can be enhanced greatly. For example, Zhang et. al. printed serpentine AgNP structures and compared them with straight lines in terms of stretchability. They found that the serpentine structure with an arc diameter of 1600 μm exhibits much higher stretchability (>25% strain with resistance change ~10 folds) than the straight line (<2% strain with resistance change ~ 10^{10} folds) [81]. Among all metals, silver has the highest thermal conductivity of 427 W m^{-1} K^{-1} at 298 K and electrical conductivity of 62.9 × 10^6 S m^{-1} at 293 K [82]. Commercially available single element metallic NP inks contain AgNPs/flakes are the most commonly used for 3D printing. These inks typically mix AgNPs with polymer additives to adjust the rheology properties and the viscosity to adapt to 3D printers such as inkjet and aerosol jet printers. Specific rheology enables the ink to transit between fluidic behavior and solid behavior, which ensures the 3D shape retention after printing due to the increased rigidity of ink coming from the shear thinning effect of the polymer. After the printing of AgNP patterns, sintering with a temperature ranging from 100 to 300 °C is usually needed

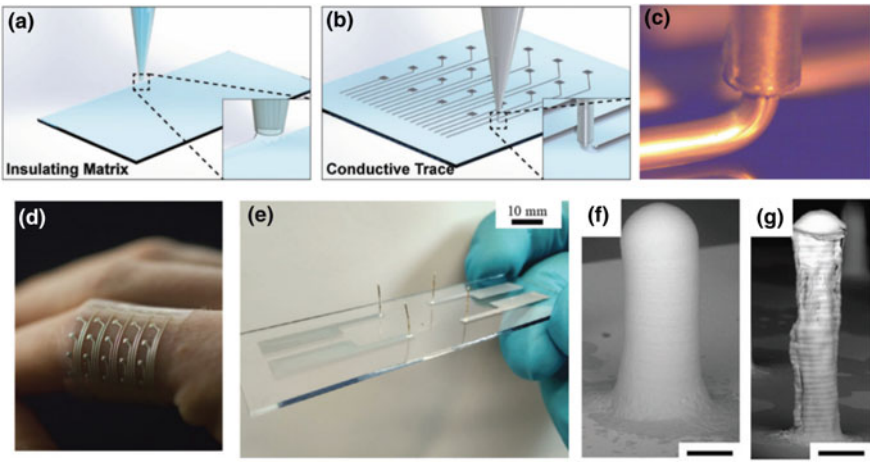

Fig. 1.5 **a** Direct ink writing of insulating matrix for the device body and B) conductive Ag/TPU traces for the sensing part [86]. **c** Image of direct writing of Ag/TPU ink through a 200 μm nozzle (scale bar 200 μm) [86]. **d** Image of a soft sensor array [86]. **e** Four printed and sintered silver pillars using the silver NP ink [87]. **f** A printed pillar with 48 layers when as-printed (not sintered) and **g** after sintered [87]

to enhance the conductivity and robustness [83–85]. Valentine et al. used DIW-based 3D printing to print both the insulating layer and the conductive layer to fabricate sensors and interconnects in a wearable electronics system, as shown in Fig. 1.5a, b [86]. The conductive ink in this work is the composite of Ag flakes and TPU, as shown in Fig. 1.5c. After the printing and the evaporation of the solvent, conductive electrodes made of a percolating network of silver flakes with a linewidth as small as 100 μm can be realized, as shown in Fig. 1.5d. Sowade et al. printed vertical 3D multilayer pillars as interconnectors by inkjet printing to achieve vertical integration of the circuit [87]. The maximum aspect ratio of the 3D-printed pillars can be up to 50:1, as shown in Fig. 1.5e. The as-printed patterns need post-process to dry and sinter the NPs, which will cause shrinkage of the pillars, as seen in Fig. 1.5f, g.

Metal nanowires (NWs) such as AgNWs [88–90], AuNWs [91], and CuNWs [92] are frequently used in electrodes for wearable electronics. Compared to NPs, NWs are more effective in forming conductive pathways according to the percolation theory [89, 93]. These percolated conductive pathways can maintain the electrical stability when the electronics are deformed [94–96]. However, 3D printing of 1D nanomaterials such as NWs is more challenging than NPs due to the severer agglomeration problem. The 3D printing technique that is applicable to NWs is extrusive-based printing. It requires the inks to have proper rheological properties and viscosity to achieve printability. The viscosity of a printable ink for extrusive-based printing such as inkjet printing, aerosol jet printing, and EHD printing ranges from 10^{-3} Pa·s to 10^{1} Pa·s. A large number of polymer additives need to be added to the ink to stabilize the NWs (i.e., reducing the agglomeration) and to increase the viscosity, which

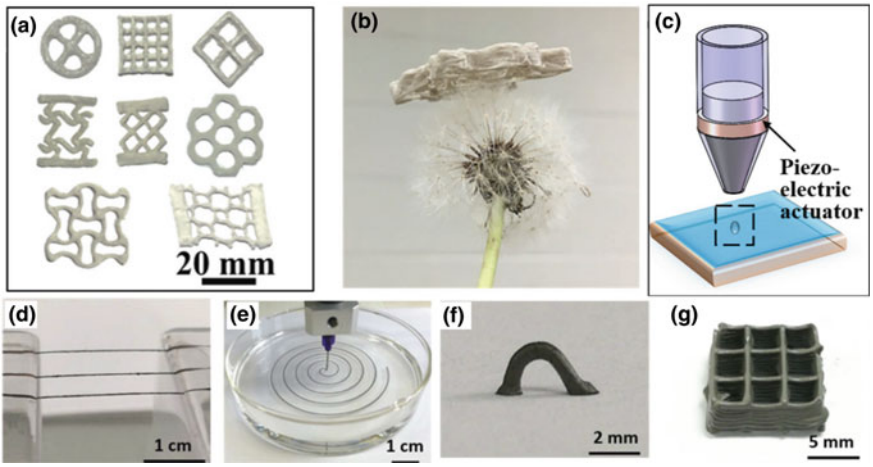

Fig. 1.6 **a** 3D-printed silver NW aerogels architectures [97]. **b** Printed silver NW aerogels standing on a dandelion [97]. **c** 3D printing setup for silver NW aerogels printing [97]. Photographs of **d** suspended microfibers, **e** coiled microfiber, **f** arch-like structure **e** and **g** scaffold structure printed using the NW gel [98]

may need harsh post-treatment including high temperature and repeated washing to remove the additives and improve the conductivity.

3D-printed AgNW aerogel was developed by Yan et al., allowing printing of ultralight rasterization structures, as shown in Fig. 1.6a, b [97]. In the printing system, an inkjet printer in a drop-on-demand mode with a piezoelectric actuator, as shown in Fig. 1.6c, is integrated with a freeze casting environment, which enables the in-situ freezing solidification of printed structures. The temperature of the freezing process highly influences the microstructure of the aerogel, where −10 to −50 °C is a proper temperature range to form tunable, uniformly thin AgNW compartments. Then, a further freezing process under a temperature of −70 °C is carried out to remove the water in the ink by sublimation. The printed AgNW aerogel is cross-linked by PVA additive in the ink, which contributes to the stable mechanical properties during bending, while sacrifices the conductivity of the printed structure. The aerogel AgNW with a density of 1.3 mg cm^{-3} only exhibited a conductivity of 1.3 S cm^{-1}, which is orders of magnitudes lower than that of the bulk silver. Instead of using polymer to crosslink AgNWs for reliable structure retention, Liu et al. developed a general strategy to make NW inks printable by gelling the NWs by 2D nanosheets including single-layer graphene oxide (GO) and titanium carbide $Ti_3C_2T_x$ (MXene) [98]. AgNW, manganese oxide (MnO_2) NWs, and zinc oxide (ZnO) NWs are successfully gelled with sufficiently high viscosity for 3D printing. Several printed structures including suspended microfibers, coiled microfiber, arch structure, and matrix structure are demonstrated, as shown in Fig. 1.6d–g. With this strategy, the conductivity of the self-standing structure can be improved to 10,000 S cm^{-1}.

1.3.2.2 Molten Metal and Liquid Metal

To achieve the high electrical conductivity needed for wearable electronics, 3D printing of molten metal with a low melting point [99] (e.g., Field's alloy and Wood's alloy) and liquid metal with a melting point at room temperature [100] (e.g., EGaIn) are emerging. Field's alloy has a melting point of 62 °C and Wood's alloy has a melting point of 70 °C. With a heater included in the 3D printing system, these alloys can be melted in the nozzle and printed out into the ambient environment, and then solidify at room temperature. Han et al. used an electrohydrodynamic (EHD) printing system (Fig. 1.7a) to successfully print molten metals (e.g., Field's metal, Wood's metal, and solder) with 3D structures [101]. The resolution can be as low as 50 μm. This is attributed to the Taylor cone formed at the tip of the nozzle under the electric field, which makes the diameter of the flow during printing much smaller than that of the nozzle. Metal trace, two-layer scaffold structure, vertical metal wire, thin wall, and metal bridge structure are printed to demonstrate the promising application of 3D fabrication for wearable electronics, as shown in Fig. 1.7b. Furthermore, the molten metal-based conductive traces encapsulated in an elastomer show self-healing properties by simply heating the device to the melting temperature of the molten alloy, as illustrated in Fig. 1.7c [99]. The required temperature for self-healing is as low as 75 °C so that they would not result in damages to the other components in the devices. However, molten metals are solid at room temperature, meaning that the

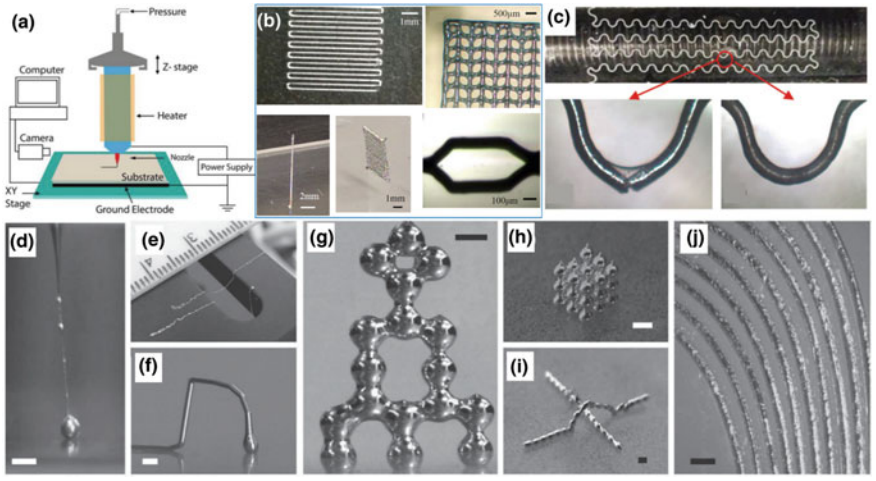

Fig. 1.7 **a** Schematic of the EHD printing system with a heater. **b** EHD printed molten metal 3D structures [101]. **c** Optical images of a local failure before and after healing [102]. The optical images of 3D-printed liquid metal with **d** thin wire shape, e free-standing wires between the gaps, **f** a free-standing liquid metal arch, **g** a tower of liquid metal droplets, **h** a 3D cubic array of stacked droplets, **i** a metal wire and an arch composed of liquid metal droplets, and **j** an array of in-plane lines. Scale bars 500 μm [45]

printed conductive traces are not stretchable. To fabricate stretchable wearable electronics, the printed patterns need to be carefully designed by a structural strategy so that the strain could be accommodated by the stretchable structures.

On the other hand, liquid metals with lower melting points remain at a liquid phase at room temperature, making them strain insensitive. So, the mechanical properties depend on the substrate material or encapsulation material but not the liquid metal itself. By choosing the proper stretchable substrate and encapsulation layer, the whole device can be stretchable. Liquid metal has been widely used as electrodes or interconnects for wearable electronics. However, facile and scalable fabrication is still needed. 3D printing technology has proven feasible to pattern free-standing 3D structured liquid metal at room temperature [45, 103]. A passive oxidation layer forms on the surface of the liquid metal pattern when the ink is exposed to air, which is key to maintaining the printed structure. This oxidation layer would not affect the conductivity of the liquid metal structure due to its thin feature on the scale of 1 nm. Extrusion, fast expelling, stacking, and sacrificial microchannel are four typical ways to 3D print liquid metal. Structures including self-standing vertical wires, stacked droplets, and bridges have been printed successfully using these methods, as shown in Fig. 1.7d–i. By controlling the diameter of the printing nozzle and the printing speed, the resolution of the printed trace can be controlled, as low as <2 μm [45].

1.3.3 Carbon-Based Materials

Carbon-based materials such as CNTs [22, 104–109], graphene (i.e. graphene oxide (GO) and reduced graphene oxide (rGO)) [110–114], graphite [115, 116], and carbon black [117–119] are emerging as functional materials in wearable electronics. They possess outstanding merits in electrical conductivity, mechanical robustness, chemical stability, and thermal properties, and are easy to be modified. Printing methods such as inkjet printing, screen printing, and direct writing printing have been used to print 2D patterns using these carbon materials. However, 3D printing of carbon-based materials is still challenging especially in terms of electrical conductivity, because typically polymer additives need to be added to the ink to maintain the structure of the printed 3D patterns, which deteriorates their conductivity. How to print stable 3D structures with high-concentration conductive carbon fillers is an urgent issue that needs to be addressed. In this section, 3D printing techniques for fabricating wearable electronics using representative carbon materials will be reviewed. The printing performances will be discussed.

1.3.3.1 CNTs

CNTs have been widely used in soft wearable electronics due to their unique 1D microstructure. Their high conductivity and robust mechanical properties make

them emerge as a promising conductor or semiconductor material for soft wearable devices. The elastic modulus and strength of CNTs are on the order of 1.0 TPa and 50 GPa, respectively [120, 121]. Similar to metal NWs, the random or aligned percolation network formed by CNTs can provide robust conductive paths, even when stretched. This makes CNTs a promising candidate as the functional parts in wearable electronics where stretchability is needed. The electrical conductivity of single-walled CNTs can be as high as 10^6 S cm^{-1}, while it is only on the order of 10^4 S cm^{-1} for multi-walled CNTs [122–127]. This level of conductivity is usually several orders of magnitude lower than that of metals; it is desirable to increase the conductivity of the printed CNT structures in order to have them as substitutes for metal electrodes.

CNTs are usually fabricated into conductive traces, bridges, matrices, and other structures to act as conductors for the electrodes and interconnect in wearable electronics [104, 105, 128–132]. 3D printing technology provides a way to improve the printability of complex 3D structures used in emerging wearable electronics, further expanding the application of these devices in the area of healthcare [22, 107], human–machine interface [133, 134], and body motion detection [106]. To print 3D-structured CNTs instead of 2D patterns, a variety of polymer materials such as polyvinylpyrrolidone (PVP) [129], PVA [135], poly(glycerol sebacate) (PGS), photopolymer [33], cellulose [105], and elastomer [47, 68, 136] have been used as the matrix or dispersion agent. These additives can improve the printability and structural stability of the CNTs for 3D printing but decrease the conductivity of the printed structure. The most straightforward method to improve the conductivity of printed CNTs/polymer composite is to remove the polymer and the solvent in the printed patterns via post-processing. Kim et al. used PVP to disperse multi-walled CNTs in water uniformly to achieve a no-back-pressure 3D printing of complex conductive structures, including freestanding pillars, bridges, and wall architectures, as shown in Fig. 1.8a–c [129]. The conductivity is improved by a thermal annealing process with a temperature of 450 °C to remove the PVP. The printing is enabled by glass micronozzles with diameters from 8 to 30 μm, and the extrusion of the ink is achieved by capillary force instead of back pressure because of the low viscosity of the ink. Accurate three-axis stepping motors with a resolution of 250 nm are used to control the printing process, which allows the printer to print structures not only on planar but also on the curved surface, as shown in Fig. 1.8d. They demonstrated a gas sensor, a point emitter, and an RF inductor printed by this system with 3D structures, which can be potential used as components in wearable electronics.

While this thermal annealing process can enhance the conductivity of the printed patterns, the conductivity of the above CNT structures can only achieve ~2540 S m^{-1} with 75% CNTs content, which is much lower than metal-based materials and the pure CNTs. Furthermore, the high temperature used to remove the polymer may destroy the other components in the soft devices such as polymer substrates. The improvement of conductivity of the 3D-printed CNTs still needs to be addressed for the large-scale applications of 3D CNT structures as conductors in wearable electronics. Nevertheless, 3D-printed CNT structures can be widely used in scenarios

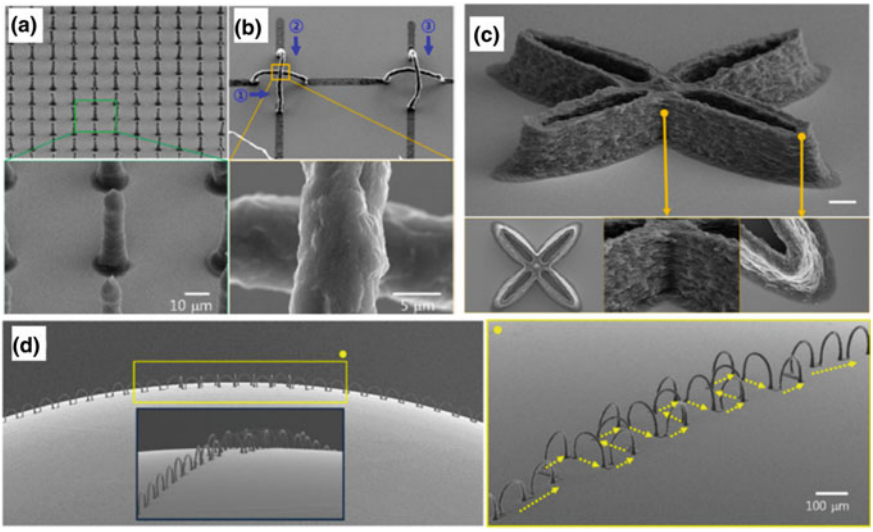

Fig. 1.8 **a** FE-SEM image of an array of free-standing CNT pillars. **b** FE-SEM image of a suspended junction pattern consisting of CNT bridges and straight lines. **c** 3D cross-shaped wall structure. All scale bars are 20 μm. **d** FE-SEM images of a concatenated CNT bridge-line structure on a curved glass substrate with an 8.4 mm curvature radius [129]

that do not request very high conductivity, such as pressure sensors [33, 68], strain sensors [136], supercapacitors [135], and triboelectric nanogenerators [137].

1.3.3.2 Graphene-Based Materials

3D printing of graphene-based materials such as GO and rGO has been attracting more and more attention recently, attributed to the increasing exploration of the applications of graphene in various areas. Soft wearable electronics is one of the most promising application that may take advantage of the excellent electrical, mechanical, and thermal properties of grapheme [138, 139]. As a typical 2D material, graphene can form percolation networks for the conductor or semiconductor building blocks in wearable electronics, such as sensors [140, 141]. Interconnects [142]. Transistors [143, 144], optical devices [145, 146], energy devices [147], etc. The development of 3D printing technology makes the manufacturing of customized structures possible for graphene-based electronics, facilitating the application of 3D-printed graphene in wearable electronics.

Similar to other nanomaterials, one common strategy to fabricate graphene-based electrodes is to mix graphene materials with a polymer matrix and print desired structures with direct writing-based 3D printing methods. By mixing graphene with PDMS elastomer with controlled weight ratio to adjust the rheological properties, a 3D printable ink was developed to fabricate scaffold structure for ultrasensitive

soft strain sensors, as shown in Fig. 1.9a, b [69]. Higher graphene ratio leads to high viscosity, which may make the printer hard to extrude the ink, while the 3D structure cannot be maintained well after printing if the graphene ratio is too low. Apart from the application for wearable soft sensors, 3D-printed graphene scaffold was also used as bioelectronics for tissue regenerative engineering [148]. The device was fabricated by extrusion-based layer-by-layer printing of graphene/polylactide-co-glycolide (PLG) composite ink, which is conductive, mechanically robust, and biocompatible, as shown in Fig. 1.9c. Different annealing temperatures after the printing were proven to have a significant influence on the mechanical properties of the printed structure. With the increase in the annealing temperature, the printed scaffold becomes more

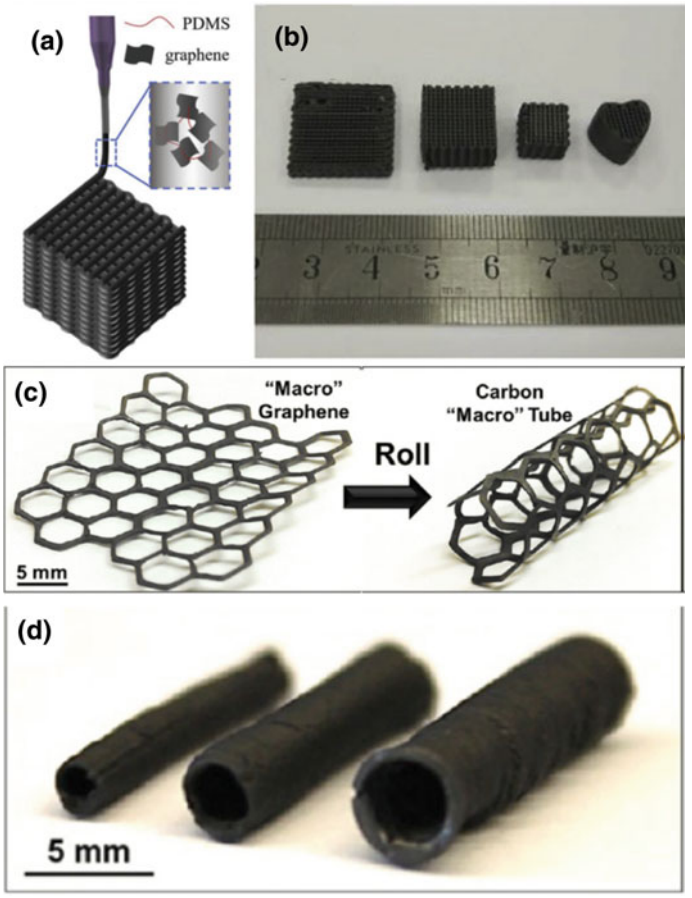

Fig. 1.9 **a** Schematic showing preparation of 3D graphene-PDMS. **b** Various 3D graphene-PDMS samples with different shapes and sizes [69]. **c** Photographs depicting that thin three-dimensional graphene-PDMS sheets are flexible and can be rolled into more complex 3D forms. **d** Various sizes that could serve as custom-sized nerve graft conduits [148]

and more brittle and undergoes brittle failure upon compression when the temperature exceeds 150 °C, due to the decomposition of PLG. In vitro and in vivo experiments found that the printed graphene scaffold can support tissue regeneration without an inflammatory response. The high programmability and resolution (~100 μm) also make it potentially applicable for precision surgical procedures, as demonstrated in Fig. 1.9d.

Graphene-based materials are also widely used as the building block of hybrid inks to enhance the mechanical, electrical, and thermal properties. Commonly used materials that are incorporated with graphene materials for 3D printable inks include conducting NPs [139, 149]. dielectric particles [150], CNTs [139], 2D MoS_2[139], and so on. For example, GO NPs were added into NP inks with PU as the binder for 3D printing of piezoresistive strain sensors [149]. Attributed to the 2D nature of GO, this sensor can work under compression and tensile strain up to 160% with a high gauge factor of 48.2. As shown in Fig. 1.10a, the GO nanoplate networks can maintain conductive paths under large stretching. The printed 3D sensor is used to detect pressure from touching of fingers (Fig. 1.10b, c). A tensile strain sensor was also demonstrated to show the high sensitivity, high stretchability, and excellent durability of the sensor. Based on this concept of hybrid 2D graphene materials with other low-dimensional materials including 0D, 1D, and 2D materials, 3D printing of GO-based aerogel hybrid with mixed-dimensional nanomaterials was achieved using a DIW printing method [139]. Benefitted from the unique structure of 2D GO nanosheets, these inks composited of GO and nanoparticles/nanotubes/nanosheets do not need polymer as the binder due to the mild crosslinking process of GO nanosheets, as shown in Fig. 1.10d. This avoids the harsh post-processing needed in most other composite inks, which may damage the printed structure or the matrix. The hybrid composites can also be printed on a curved surface, as shown in Fig. 1.10e, which is of great interest to conformal contacted wearable electronics.

1.3.4 Polymer Materials

1.3.4.1 Conductive Polymer

Conducting polymers are intrinsically conductive. They have been widely used in a variety of promising applications including wearable electronics, biosensors, energy storage devices, optoelectronics, etc. [151–153]. These materials possess unique properties (e.g., mechanical, electrical, thermal, and optical properties) of polymers. Furthermore, they are usually chemically stable and biocompatible, which makes them promising candidates for implantable and epidermal wearable electronics. It is of great importance to fabricate conductive polymers into diverse structures to meet the mechanical and electrical requirements for different applications. Conventional manufacturing of conductive polymers mainly includes drop casting, spin coating, ink-jet printing, screen printing, aerosol printing, and lithography. However, limitations exist when using these techniques to fabricate complex

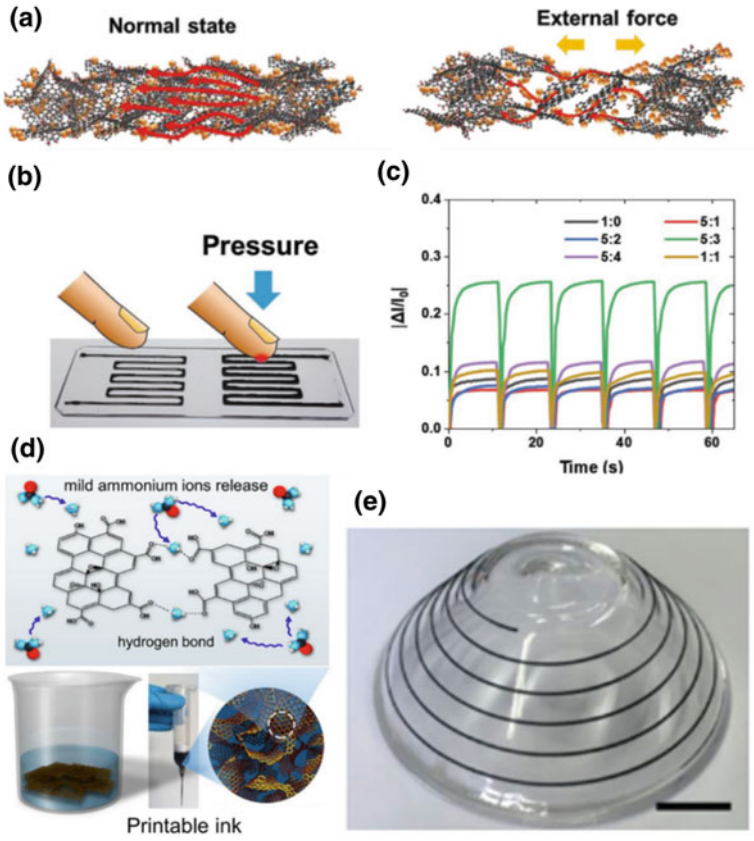

Fig. 1.10 **a** Schematic illustration of the sensing mechanism for pressure sensor fabricated by GO and NPs. **b** Schematic showing pressure sensing. **c** The current change when the pressure sensor is pressed with various weight ratios between GO and NPs [149]. **d** Schematic diagram of printable cross-linked graphene ink. **e** 3D-printed hemispherical spiral using the GO/Ag hybrid ink [139]

structures with high resolution, high aspect ratio, or curved surfaces. 3D printing techniques can potentially address these issues. Poly [3, 4-ethylenedioxythiophene]: polystyrene sulfonate (PEDOT:PSS), as one of the most widely used conductive polymers, has been used in 3D printing to fabricate wearable optoelectronic [154], thermoelectric [155], and bioelectronic [154] devices. To realize the printability of PEDOT:PSS, Yuk et al. developed a high-performance 3D printable ink [154]. The paste-based conducting polymer ink is prepared by cryogenic freezing of aqueous PEDOT:PSS solution followed by lyophilization and controlled re-dispersion in water and dimethyl sulfoxide (DMSO) mixture. To make the ink with suitable rheological properties, relatively high concentration PEDOT:PSS (5–7 wt%) was added to the solvent to transform the ink from low viscosity liquid to gels with the shear-thinning property. Conducting meshes fabricated by multilayer printing

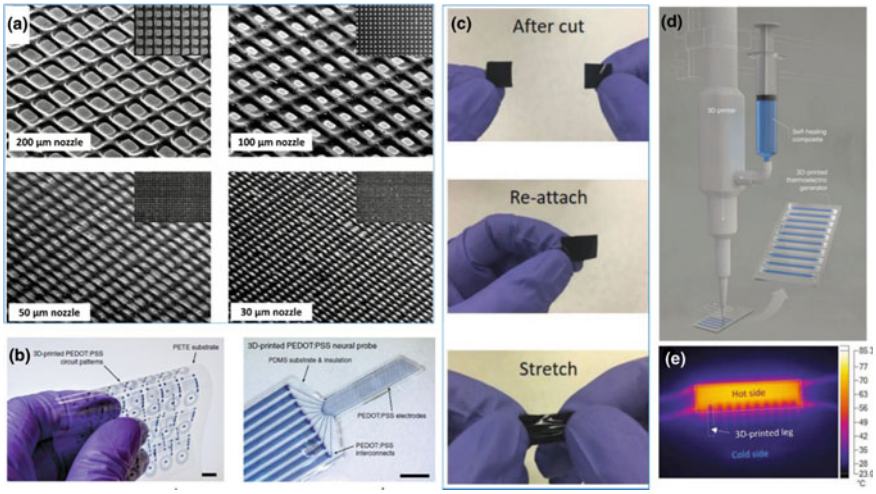

Fig. 1.11 **a** SEM images of 3D-printed conducting polymer mesh. **b** Bending of the 3D-printed conducting polymer circuit without failure (left) and the 3D-printed soft neural probe in magnified view (right) [154]. **c** Photographs showing the composite film after cut, reattach, and then stretch. **d** Schematic of the 3D-printer setup and printing process for PEDOT:PSS composite. **e** An example of infrared thermal image of the ten-leg composite film thermoelectric generator [155]

of PEDOT:PSS was demonstrated with resolution as high as 30 μm, as shown in Fig. 1.11a. High-density flexible electronic circuit patterns (Fig. 1.11b) were 3D-printed using this ink and applied to bioelectronics applications as an implanted probe.

Wearable thermoelectric generators were fabricated by 3D printing of PEDOT:PSS composite to harvest low-grade heat from the human body and convert it into electricity [155]. With polymeric surfactant Triton X-100 added as a healing agent, the printed composite structure can not only bear a 35% strain without decrease in electrical conductivity and Seebeck coefficient, but also self-heal after being cut, as shown in Fig. 1.11c. A ten-leg composite film electrically connected in series and thermally in parallel was printed to investigate the power generation of the thermoelectric generator (Fig. 1.11d and e). The thermoelectric generator provides a maximum output power of 12.2 nW and can retain over 85% power output after self-healing from a mechanical cut. The 3D printing technique makes the fabrication of composite structures all solution-based and facile for large-scale manufacturing.

Apart from printing 3D structures directly, another category of 3D printing is printing patterns or structures on a 3D surface such as concave/convex hemispherical surface and step-shaped surface. Polymer photodetector arrays were successfully printed on both the planar surface and the inner face of a hemispherical surface, as shown in Fig. 1.12a and b [156]. The single photodetector is fabricated by 3D printing of different materials including poly [3-hexylthiophene] (P3HT) photoactive layer, PEDOT:PSS transparent anode, EGaIn liquid metal cathode, and AgNP interconnect layer-by-layer (Fig. 1.12c). The one-pot 3D printing platform makes the fabrication

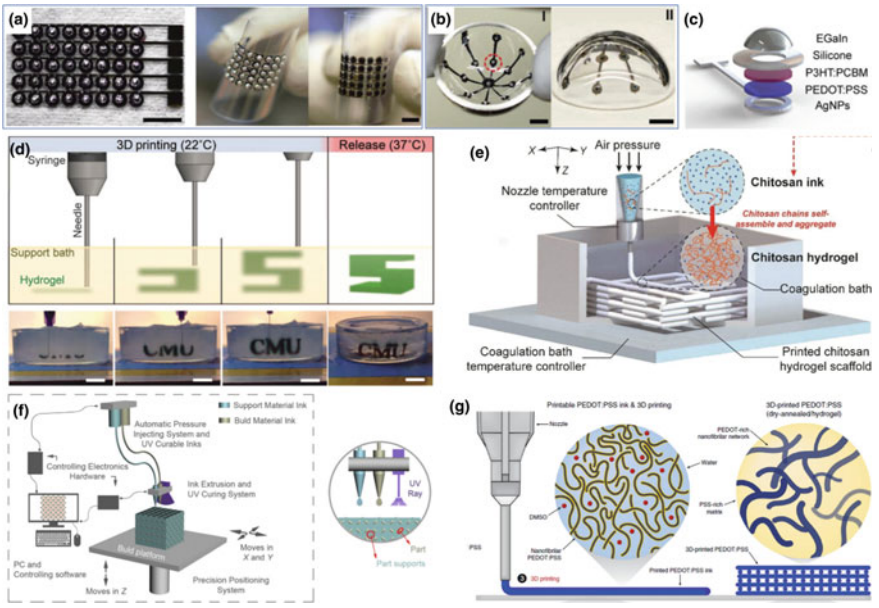

Fig. 1.12 **a** photodetector array printed on PET when flat (left) and bent (right). **b** Photographs of the photodetector array printed onto the inner surface of a hemispherical glass dome. **c** Schematic diagram of the structure of the photodetector [156]. **d** Schematic of printing the hydrogel precursor into a supporting solvent [157]. **e** Schematic of printing the hydrogel precursor into a reaction solution that can solidify the hydrogel in-situ [161]. **f** Schematic of 3D printing process of UV curable ink [30]. **g** Schematic of the set up for directly printing PEDOT:PSS hydrogel without external assistance [154]

of multi-material systems more efficient and facile. Different nozzles were used on the same printer to print different inks, with proper printing parameters, for layer-by-layer fabrication of the photodetectors. The capability of printing photodetectors on a hemispherical surface makes it possible to be integrated into a "bionic eye" vision system.

Besides the intrinsically electrical conductive polymers, hydrogels, a type of ionic conducting polymers consisting of a large amount of water, salt ions, and cross-linked polymer frameworks, are emerging for applications in soft wearable electronics. 3D printing of these hydrogels enables fast prototyping of soft biomedical devices that can be mounted on the skin or inside the body for applications like portable patient monitoring, wound treatment, and tissue/organ engineering. Due to the solidification requirement of the hydrogel during or after printing, there are generally four strategies for printing hydrogel structures. (1) Printing the hydrogel precursor into a supporting solvent such as hydrophobic fluids, thermoreversible fluids, and thixotropic materials, or supporting field such as electric field, to fix the shape of the hydrogel precursor first [157, 158]. After the printing, the hydrogel precursor is solidified by stimulation and the supporting solvents or field can be removed, as shown in Fig. 1.12d. When

printing into the supporting solvent, the support bath should have rigid behavior at low shear stresses but can flow at higher shear stresses. When the extrusion nozzle moves in the bath, there is little mechanical resistance; the hydrogel being extruded out of the nozzle and deposited within the bath is held in place. The bath can be gelatin [157]. mixture of alginate and methylcellulose [159]. or laponite suspension [160]. Complex structures including helix, flowers, and human brain model can be printed by this method [157, 159]. The advantage of this support-bath method is that the hydrogel can be solidified either during the printing or after the printing. But removal of the supporting liquid or field makes the method not applicable for hollow structures. (2) Printing the hydrogel precursor into a reaction solution that can solidify the hydrogel in-situ, as shown in Fig. 1.12e. [161] The hydrogel precursor ink changes its rheological property once it meets the reaction solution so that the structures form as soon as the extrusion of the ink. For example, increasing the temperature of the coagulation bath when extruding a chitosan ink can stimuli the self-assembly of chitosan chains, so that regenerated nanofibers can construct hydrogels [161]. This method enables fast solidification of the hydrogel but may encounter problems on limited ink and reaction solvent selections. (3) Using fast cross-link stimulations such as UV light and heat to solidify the hydrogel during the patterning or right after the extrusion [30, 31, 34, 162–164], with examples shown in Fig. 1.12f. The resolution and quality of the printed structure highly rely on the curing speed. With fast curing, resolution of the printed features can reach 140 μm [162]. More complex structures with the shape of snowflake and butterfly can be printed. But these procedures usually have the problem of clogging nozzles when being used in a direct writing printing system. (4) Directly printing the self-standing hydrogel structures without external assistance [64, 65, 154, 165]. such as the process shown in Fig. 1.12g. For example, PAAm-based hydrogels were modified by Carbomer to enable self-standing after printing, where Carbomer acted as a rheology modifier in the ink [65]. This method can address the issue of structure fidelity and nozzle clogging. But challenges have risen in developing hydrogel inks and tuning printing parameters.

1.3.4.2 Shape Memory Polymer

Shape memory polymers (SMPs) are smart stimuli-responsive polymeric materials that can memorize permanent shapes and recover from temporary shapes to permanent shapes under external stimuli, such as temperature, electric potential, light, etc. [166]. The thermally induced shape memory behavior requires two critical temperature: a lower temperature where chemical or physical crosslinks occurs to set the permanent 3D shape, and a transition temperature to control the molecular switching segments that fix the temporary shape. When the material is deformed above the transition temperature, the temporary shape is obtained. Then the material will recover to its permanent shape when the temperature is reduced below the transition temperature [38]. When the SMPs are used as the functional materials in soft wearable electronics, they not only satisfy the material requirements of conventional soft electronics, but also bring some special features that traditional polymers do not possess,

such as shape memory effect, self-healing capability, and variable elastic modulus. These unique properties along with the high stretchability and low cost of SMPs make them more and more popular in the application of wearable electronics. 3D printing of SMPs further benefits the application of the materials in various fields by reducing the fabrication steps/time and increasing the programmability of the structure.

One of the widely used SMPs is polycaprolactone (PCL) based semicrystalline polymer. Zarek et al. developed a general 3D printing method that can print PCL macromonomer through stereolithography 3D digital light processing (DLP) printer with UV light as the solidification stimuli [38]. Attributed to the shape memory property of the printed structure, the system was used to print a 3D structural electric circuit with the shape memory parts as switches. As shown in Fig. 1.13a, the

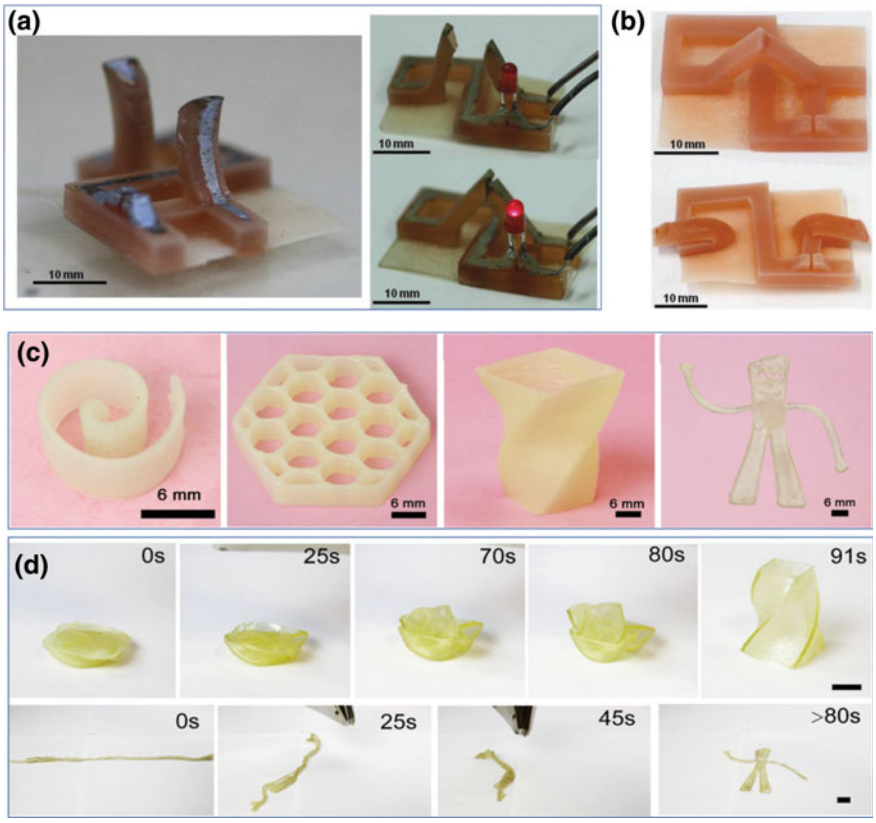

Fig. 1.13 **a** 3D-printed shape memory construct (left) in its off state (right top) and on state (right bottom). **b** A 3D-printed construct (top) programmed into its temporary state to enable inkjet printing on a 2D surface (bottom) [38]. **c** 3D structures by 3D printing of self-healing SMP. **d** Recovery of the printed SMP structure after compressed and stretched. All the scale bars are 6 mm [167]

temporary shape is an open electrical circuit, and when heated above the transition temperature, the circuit closes and turns on an LED. Furthermore, the circuit is printed at a temperature above the transition temperature, which may transform the printing of the 3D structure into a simpler 2D structure, shown in Fig. 1.13b. This strategy reduces the size of the unused devices and avoids using a complex 5-axis printing system. Such responsive printed structures have the potential to be used in soft robotics, minimally invasive medical devices, sensors, and wearable electronics [38].

Kuang et al. use 3D printing to print a self-healable shape memory polymer [167]. A highly stretchable semi-interpenetrating polymer network elastomer with an embedded PCL was printed using the DIW approach. The PCL provides both the self-healing and shape memory properties for the printed structure. Archimedean spiral, honeycomb, hollow vase, and Gumby model were printed using this system, as shown in Fig. 1.13c. Attributed to the shape memory property, the printed structure can be fully recovered from stretched and compressed state to the original shape (Fig. 1.13d). Moreover, the printed structure can self-heal after being cut repeatedly, despite with some mechanical property deterioration.

1.3.4.3 Soft Substrate

Although 3D printing of various functional materials and even polymer composites has been investigated to achieve the fast and reliable fabrication of wearable electronics, 3D printing of soft substrates is still needed to further improve the prototyping speed and quality, especially in an all-printed system. Traditional thermoplastic and thermoset polymers for 3D printing such as PLA, acrylonitrile butadiene styrene (ABS), and TPU are up to four orders of magnitude stiffer than soft tissue [168, 169]. This makes them have a modulus mismatch with the human skin when used as the substrate materials for wearable electronics, leading to nonconformal contact between the device and the skin and uncomfortable wearing. Adjusting the composition of hard segments and soft segments in polymers can tailor the mechanical properties of the polymer to better fit with the human skin. For example, soft segments such as poly-(tetrahydrofuran) (PTMG), poly(propylene glycol) (PPG), and polycaprolactone diol (PCL-diol) were added to synthesize polyurethane acrylate oligomers (PUAs) for UV curable 3D patterning process to modify the tensile strength, elongation at break, and Young's modulus [37]. A homemade DLP 3D printer was used to print the modified ink layer by layer, as shown in Fig. 1.14a. The PTMG modified PUAs exhibited high transparency and the best comprehensive mechanical properties. Although the modified elastomer has higher stretchability and maintains its mechanical strength without sacrificing the elongation at break compared with original polymers, the Young's Modulus is around 6.7 MPa, much higher than that of human skin (2–600 kPa).

To address this problem, one approach is to apply 3D printing to printing soft silicone elastomer materials such as PDMS to fabricate soft substrates for wearable devices. Zheng et al. developed PDMS composite elastomer inks for DIW 3D

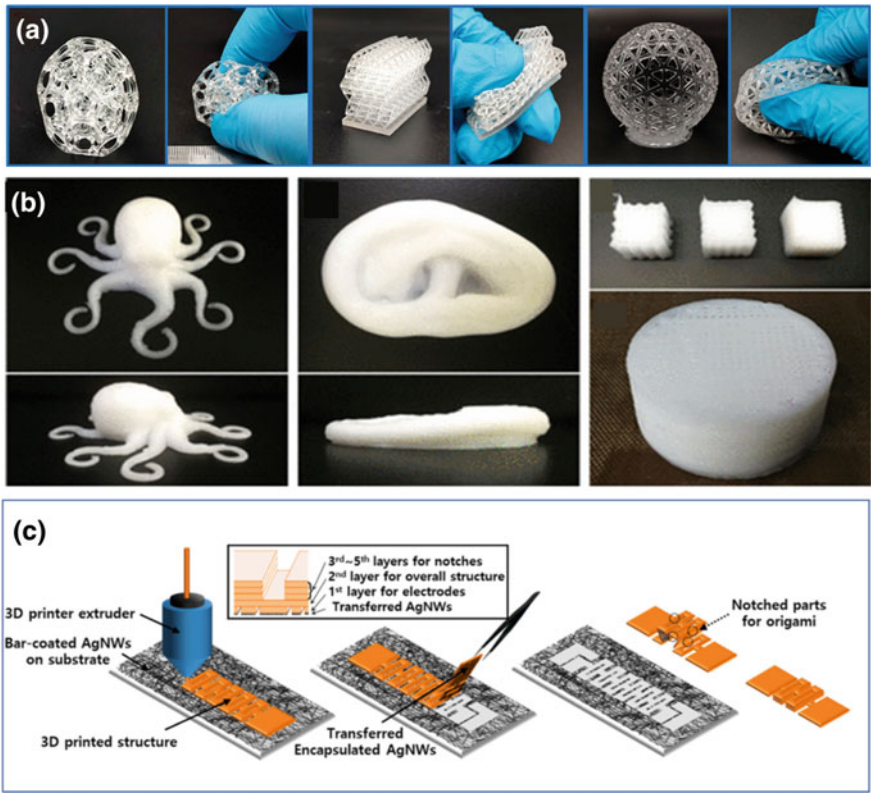

Fig. 1.14 **a** Photographs of the 3D-printed hollow PUAs 3D structure and their shape deformation with finger pressing [37]. **b** Photographs of 3D-printed PDMS/PTFE structure [170]. **c** Schematic of the 3D printer-based kirigami/origami approach combined with silver nanowires (AgNWs) [67]

printing by adding PTFE micro powder as a thixotropic agent [170]. The mechanical properties of the printed structures can be tailored by adjusting the ratio of PDMS and PTFE. An octopus model, an ear model, cubic cellular lattices with different filament gaps, and cylinder structures were printed using this approach, as shown in Fig. 1.14b. Benefiting from the increased electron affinity of PDMS by adding PTFE, a 3D-printed triboelectric nanogenerator (TENG) with a PDMS composite as the supporting structure and friction layer was fabricated. TENG works by cyclic compressing-releasing and is self-recoverable. Light-emitting diode (LED) arrays were successfully lighted by manually pressing TENG, demonstrating the good output performance of the fabricated TENG.

Another approach to enhance the wearability of the device is to print structurally designed patterns with high stretchability that can adapt to the movement of the human body. A 3D printing strategy was developed to fabricate kirigami/origami-based 3D structure with extreme stretchability and high areal coverage [67]. The

Table 1.1 Mechanical properties of representative 3D-printed soft substrates compared to human skin

Material	Printing technique	Young's modulus (kPa)	Stretchability (%)	Reference
Human skin	–	2–600	100	[5]
TPU	FDM	–	440	[67]
PDMS/PTFE	DIW	156	483	[170]
SMP	DIW	400	500–600	[167]
PBSF-FA-BMI	DIW	1870 ± 80	300–400	[171]
PDMS	FDM	1200 ± 100	130	[169]
PUAs	DLP	6700 ± 700	414.3 ± 7.6	[37]

PBSF-FA-BMI: poly(butylene sebacate-co-butylene fumarate) functionalized with furfurylamine (FA) and cross-linked with bismaleimide (BMI); PUAs: polyurethane acrylate oligomers

fabrication procedure is shown in Fig. 1.14c. TPU was printed by the FDM mechanism with an extruder onto a substrate covered with AgNW network. After the TPU is cured and detached from the substrate, the AgNW network is embedded under the surface of the TPU substrate, exhibiting outstanding conductivity. Furthermore, attributed to the programmability of the 3D printing system, notches can be designed in the printed kirigami pattern and assist the forming of origami structure by folding the 2D kirigami patterns into multilayers, as shown in Fig. 1.14c. This method was then used to fabricate high-area-coverage solar cell arrays with a designed bridge-island structure (Table 1.1).

1.4 Application of 3D-Printed Wearable Electronics

3D printing technology provides reliable solutions to facile fabrication of wearable devices. Due to the capability of printing solution-based materials, bottom-up fabrication of micro/nano-materials can be achieved by a 3D printing system. Moreover, polymer materials with proper rheology properties, thermoset/thermoplastic properties, and optical solidification response can be printed into customized structures more easily with higher product quality using 3D printing than conventional approaches such as laser cutting, injection molding, and soft lithography. Advances in functional materials have facilitated the ever-increasing performance of wearable sensors. However, the fabrication processes adapted to these functional materials still need further investigation. Considering that the most important building blocks of soft wearable electronics are functional materials and polymer substrates/encapsulations, 3D printing possesses a great potential in fabricating such electronics for novel applications including sensors, actuators, heaters, antennas, and interconnects, among others. This section will briefly summarize 3D-printed wearable systems in these application areas.

1.4.1 Wearable Sensors

In the past decade, development of soft wearable sensors has seen tremendous progress due to the increasing interest in electronic skin, human–machine interface, health monitoring, and other applications [80, 172, 173]. In this section, applications of using 3D printing techniques to fabricate representative wearable sensors will be discussed.

1.4.1.1 Strain Sensors

Wearable strain sensors can evaluate the skin deformations and body movements. Parameters to evaluate the performance of a strain sensor include sensitivity, linearity, hysteresis, and dynamic durability. To effectively capture the deformation level or motion features, a strain sensor should meet several requirements. (1) The sensor should be highly stretchable with low Young's modulus. The high stretchability will ensure the working function under human's daily movements, which may introduce a local strain over 75% [174, 175]. The low Young's modulus is to match the mechanical property of human skin (the modulus of epidermis is 140–600 kPa, and that of dermis is 2–80 kPa) and keep conformal contacts, which is vital for signal accuracy and quality. (2) For capturing of subtle strains, the sensor should have a high sensitivity. For example, by mounting a highly sensitive strain sensor on throat, the subtle motions of throat including swallow and speaking can be detected. (3) The fabrication process is scalable for mass production. 3D printing provides reliable solutions to meet these requirements. 3D printing is compatible with complex structural designs such as kirigami, origami, serpentine shape, and island-bridge are widely used to accommodate the large strain. In addition, 3D printing of advanced materials such as NPs, NWs, and graphene can easily integrate these materials into wearable sensors and increase the sensor sensitivity. Furthermore, the facile and mature 3D printing processes are amenable to scalable manufacturing of wearable sensors with high throughput at low cost.

Strain sensors can be mainly divided into capacitive and resistive types. Capacitive strain sensors typically exhibit low sensitivity, high linearity, and negligible hysteresis. In contrast, resistive strain sensors typically show high sensitivity but suffer from large nonlinearity and hysteresis. Typical capacitive wearable strain sensors have sandwich structures with conductors as electrodes and polymer as dielectric layer sandwiched between electrodes. The gauge factors (GFs) can be calculated by

$$GFs = \frac{\Delta C}{\varepsilon C_0} = \frac{1 - \varepsilon \nu_e + \nu_d - \nu_e}{1 - \varepsilon \nu_d} \tag{1.1}$$

where ΔC corresponds to the capacitance change of sensors, ε refers to strain, C_0 is measured as the initial capacitance, ν_e and ν_d represent the Poisson ratio of the electrode and dielectric layers, respectively [5, 176]. The maximum GF is 1 according to this equation. Yin and co-workers use DLP printing technique to print copolymerize acrylamide monomers and PEGDA hydrogel [162]. $MgCl_2$ was added to hydrogel to provide ion conductivity. To fabricate a capacitive strain sensor, two printed copolymer films with multiple parallel grooves were sandwiched by three 3 M very-high-bond (VHB) tapes, as shown in Fig. 1.15a. The VHB tape acted as both encapsulation layer and the dielectric layer. The fabricated sensor can be used as both pressure senor and strain sensor, as shown in Fig. 1.15b. The pressure-dependent capacitance changes and sensitivity are demonstrated in Figure xc.

A straightforward method to fabricate resistive strain sensors using 3D printing is to print conductive materials or conductive filler/polymer composites with stretchability. When the printed structure is stretched, the elongation of the structure changes its resistance. A tough and conductive double network hydrogel was fabricated by 3D printing technology to be used as a strain sensor with rapid sensing response, high sensing stability, and high strain sensitivity [164]. A wearable resistive strain sensor was fabricated and mounted on a finger joint, which can rapidly and precisely detect the motions of finger bending, as shown in Fig. 1.15d. Gao et al. demonstrated an integrated wearable sensor array fabricated with coaxial extrusion of conductive fiber by 3D printing technology [177]. The sensor array enables strain detection and

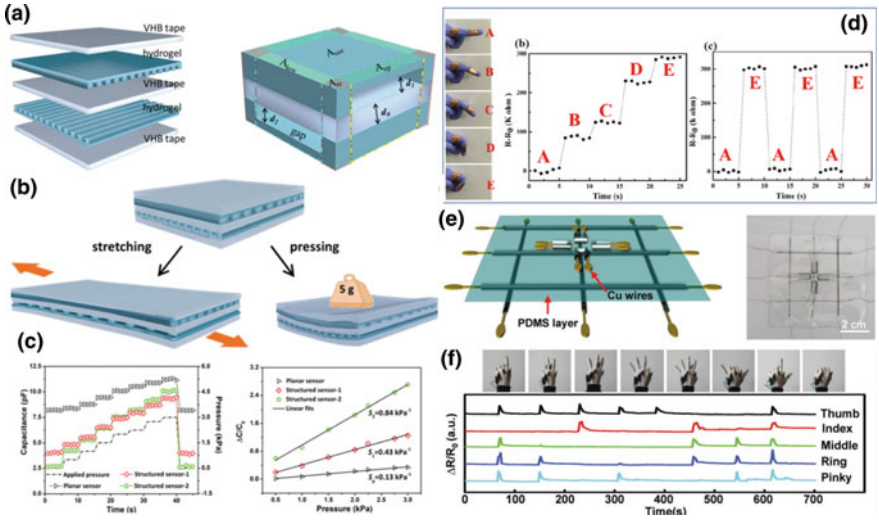

Fig. 1.15 **a** Schematical illustration of 3D-printed strain sensor by sandwiching a layer of stretchable dielectric (VHB 4905 tape, 3 M) between two layers of hydrogel film. **b** Schematic illustrations for the two sensing mechanisms of the capacitive sensor. **c** Pressure-dependent capacitance changes and sensitivity. **d** Photographs of finger bending (left) and associated resistance change of the resistive strain sensor [164]. **e** Schematic of the integrated sensor (left) and optical image of the integrated sensor (right). **f** Single-fiber strain sensors were used to identify the human hand gesture [177]

pressure detection on one platform, owing to the design of the sensor configuration. As shown in Fig. 1.15e, four resistive strain sensors in "U" shapes with a gauge factor of 11.8 were printed in the center of the array, where the gauge factor is calculated by

$$GFs = \frac{\Delta R_\varepsilon / \Delta R_{\varepsilon 0}}{\varepsilon} \tag{1.2}$$

where ε is the applied strain, ΔR_ε is the resistance at applied strain ε, $\Delta R_{\varepsilon 0}$ is the resistance when applied strain is zero, and $\Delta R_\varepsilon / \Delta R_{\varepsilon 0}$ is the relative resistance change. The strain sensor shows a small variation in resistance after repeat loading/unloading test for 10,000 cycles, exhibiting good durability for the strain sensor. As demonstrated, the strain sensors were applied to monitor human hand gestures, as shown in Fig. 1.15f.

A new method, embedded 3D printing (e-3DP), was developed for fabricating strain sensors by printing conductive carbon grease filler directly into an uncured elastomer reservoir, which was then cured to encapsulate the conductive path. The device maintains the stretchability of the elastomer matrix and exhibits high conformability. By printing the strain sensors within a pre-molded glove-shaped reservoir, an electronic glove that can capture the movement of finger joints was demonstrated, illustrating the potential of this method for fabricating soft functional devices for wearable electronics.

1.4.1.2 Pressure Sensors

Pressure sensors are a basic component for electronic skin, which can be mounted on human skin to evaluate the touch force/pressure or mounted on robotics to establish a human–machine interface. The piezoresistive type is widely used for wearable pressure sensors. The compression from an external force deforms the sensor and changes its resistance. Simply because larger deformation (under the same force) results in higher sensitivity, hollow or porous structures and scaffold structures are employed to enhance the performance of the sensor. 3D printing provides a reliable route to fabricate hollow structures, which shows promising potential to program the structure of pressure sensors. For example, Wang et al. printed 3D scaffold structured carbon black/TPU composite on silver electrodes to fabricate the pressure sensor, as shown in Fig. 1.16a [73]. Due to the unique configuration of the sensor, the tensile stress concentrates at the helix interdigital electrodes and substrate underneath the piezoresistive sensing element. The maximum stress in the sensing layer is only about 5% when the device is stretched up to 50%, which ensures the stable out-of-plane pressure response and minimized in-plane stretching interference.

On the other hand, if the Poisson's effect causes compression in the transverse direction when the sensor is stretched, the sensor can work as both the pressure sensor and strain sensor. Microstructured ionic conductive hydrogel electrodes were printed using a commercial DLP printer to fabricate a highly sensitive transparent

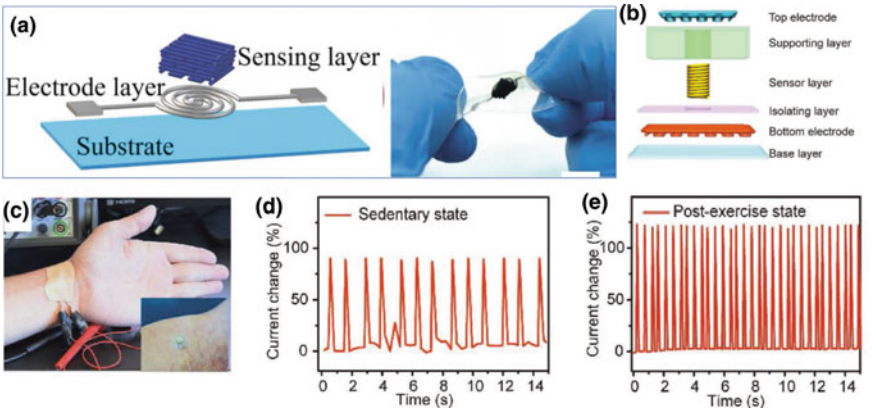

Fig. 1.16 **a** Schematic structure of the stretchable piezoresistive sensor device (left) and optical image of a representative stretchable piezoresistive sensor (right) [73]. b Schematic of the tactile sensor consisting of a base layer, top and bottom electrodes, an isolating layer, a sensor layer, and a supporting layer. **c** Photograph showing the tactile sensor mounted directly above the radial artery. Measurement signals of the radial pulse under **d** sedentary and **e** post-exercise states [72]

pressure/strain sensor [162]. The sensor is a capacitive type, where the thickness of the dielectric layer changes with the pressure, leading to a capacitance change. The microstructures on the printed electrodes introduce air gaps into the capacitor, which is critical to enhancing the sensitivity. When the sensor is pressed, the air gap and the dielectric layer shrink, the sensor works as a pressure sensor. When the sensor is stretched, the air gap and the dielectric layer are also compressed due to the Poisson's effect, the sensor works as a strain sensor [176]. 3D printing technology makes the fabrication of skin-like sensors more facile and programmable. By mounting the sensors at different locations of the human body, such as joints (e.g., finger knuckle, wrist, elbow, knee, and ankle), chest, and throat, the movement of the body, respiration, and speaking can be monitored, respectively.

Multi-material fabrication using one printing system is also a notable advantage of 3D printing. The conventional fabrication processes usually include several steps such as drop casting, spin coating, printing, and molding to complete the fabrication of one device. However, all-printed wearable electronics enabled by 3D printing of different materials by one setup have emerged. An all-printed piezoresistive pressure sensor was developed by Guo et al. with a one-step customized 3D printing process, where only the print nozzle needs to be adjusted to adapt different inks [72]. The sensor was composed of several layers including a base layer (silicone), a sensor layer (68% Ag/silicone), two electrode layers (75% Ag/silicone), an isolating layer (silicone), and a sacrificial supporting layer (40% Pluronic), as shown in Fig. 1.16b. Owing to the high flexibility, stretchability, and sensitivity of the 3D-printed pressure sensor, it was mounted at the wrist to monitor the pulse rate, as shown in Fig. 1.16c–e. Besides, pressing motion and bending motion of human fingers were also measured as

a demonstration to show the potential of the all-printed pressure sensor for wearable sensors and human–machine interfaces.

1.4.1.3 Temperature Sensors

Wearable temperature sensors can be used to monitor human health in real time by evaluating temperature variation related to some diseases such as respiration disease, hypothyroidism, diabetes, and Parkinson's disease. Several types of temperature sensors exist including thermocouples, resistance temperature detectors (RTDs), thermistors, and semiconductor sensors. To get reliable body temperature data for precise diagnosis, wearable temperature sensors should meet two critical requirements. (1) The sensor should be conformally mounted on the human body to avoid impeding the heat transfer from the human body to the sensor and minimize the influence of the ambient environment. (2) The sensor should be strain-insensitive to reduce the interference from body movement. The first issue can be addressed by soft electrodes that can adapt to the curved surface of the human body, and the second issue can be addressed by designing the stretchable sensor structure, where strain does not change the resistance [85]. 3D printing is superior in fabricating soft electrodes and complex structures, which makes it an excellent fabrication approach for wearable temperature sensors. A DIW-based 3D printing method was used to print graphene/PDMS composites to fabricate wearable RTD type of temperature sensors [178]. Three different mesh-type structural designs including grid, triangular, and hexagonal structures are constructed, as shown in Fig. 1.17a–c. Compared with the solid-type temperature sensor, the gird structured sensor exhibits much higher stability when there is an external strain applied on the sensor, i.e., body movement. Grid sensors and solid sensors were mounted on the human wrist with the resistance signal being monitored. The drift of the measured temperature is as high as 0.5 °C due to the bending of the wrist in the case of the solid sensor, while a negligible drift value of only ∼0.2% is observed for the grid sensor, under the same external deformation. 3D printing can be used to print, with high fidelity, not only temperature sensors but also other wearable sensors that need to eliminate strain artifacts with complex mechanical designs.

1.4.1.4 Pulse Oximeters

Pulse oximeter is clinically used to detect the vital signs such as heart rate and peripheral capillary oxygen saturation (SpO_2) for evaluating physiologic status of human objects, especially patients with neonates, postoperative, and cardiopulmonary diseases. With the COVID-19 pandemic spreading all over the world, wearable pulse oximeter becomes one of the most straightforward and reliable devices that can provide easy-accessed, off-clinical evaluation of the symptoms of suspected cases. Traditional pulse oximeters are bulky and rigid, causing a lot of interference when used. Lightweight soft pulse oximeter offers a great opportunity for continuous

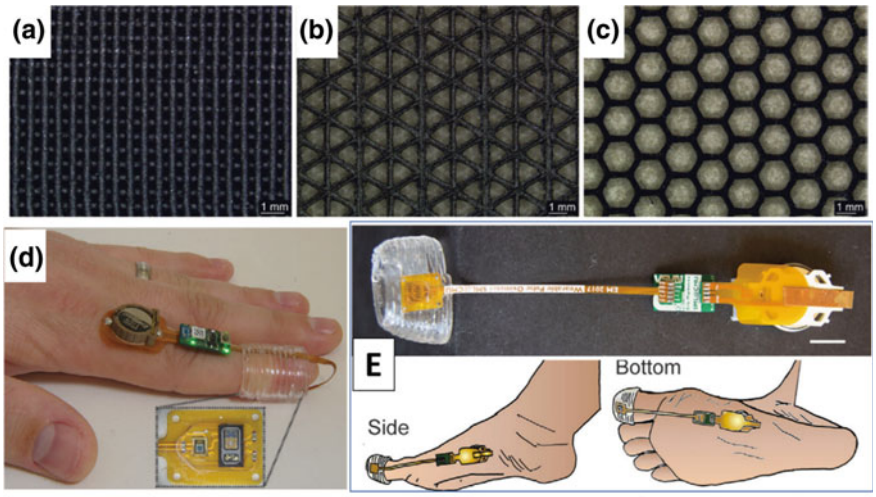

Fig. 1.17 Optical microscopy images of the 3D-printed graphene/PDMS composites with **a** grid structure; **b** triangular porous structure; and **c** hexagonal porous structure [178]. **d** Representative image of the customized wearable pulse oximeter tested on the index finger. **e** Complete wearable toe pulse oximeter and the schematic images of pulse oximeter placed on the side and bottom of the toe. Scale bar is 1 cm [169]

and remote heart rate and SpO_2 monitoring. There are typically four parts in a pulse oximeter system: light sources, photodetectors, holding frameworks, and data acquisition components. 3D printing techniques have been proven to be efficient and robust to fabricate these components. Abdollahi et al. applied freeform reversible embedding (FRE) 3D printing system to fabricate user-customizable soft pulse oximeter [169]. Like the portable pulse oximeter on the market, the soft pulse oximeter is mounted on the fingertip. However, 3D printing allows premeasure and on-demand printing of PDMS to fabricate the finger cuff for specific users, which make the soft pulse oximeter fit for fingers or toes, as shown in Fig. 1.17d, e. The toe-type sensor was tested at rest, while sitting and during walking. The human movement activity, pulse, and oxygen saturation can be monitored by the customized pulse oximeter. However, still some challenges remain in 3D printing of pulse oximeters.

1.4.2 Wearable Energy Devices

One of the key challenging issues for wearable systems is the wearable power sources. These power source devices should have a small footprint to make the system unobtrusive, and the energy they provide should be sustainable and continuous. Moreover, the power source devices should be biocompatible. This section will discuss

the research efforts on 3D-printed wearable energy systems including storage and conversion systems.

1.4.2.1 Energy Storage Devices

Basically, energy storage devices can be categorized into supercapacitors and batteries. The main building blocks in these two devices are electrodes, electrolytes, and separators. They are different in their mechanisms of energy storage. A supercapacitor relies on the mechanisms of electrical-double-layer capacitance and/or pseudocapacitance, while a battery is based on relatively slow faradaic reactions [179]. Conventional fabrication of these storage devices mainly uses 2D casting methods such as doctor blade casting. These 2D devices are bulky and nonconformal when used as wearable power sources. 3D printing can not only fabricate soft wearable energy storage devices with good conformability, but also print complex electrodes that have higher surface area for electrolyte contacting, which is conducive for increasing the capacity of the device. For example, a bracelet-shaped Li–S battery with a scaffold structure as the electrode was designed and manufactured using the DIW- (Fig. 1.18a) and FDM-based 3D printing (Fig. 1.18b) [150]. The GO cathode is printed by the DIW technique, and the battery case is printed by the FDM technique. The printed wearable battery is shown in Fig. 1.18c–e. Graphene/phenol formaldehyde (PF) resin paste was modified with SiO_2 particles to achieve the desired rheology property for printing. Attributed to the large surface area provided by the printed scaffold electrode, an interpenetrating transmission path for electrons and ions is established to enhance the charge transfer at the interface between the electrodes and the electrolyte. And the porous structured electrodes also provide the transport channels for mass transportation of Li^+ and sufficient space for the electrolyte to diffuse to the area of the electrodes. The loading density of the active materials is also improved

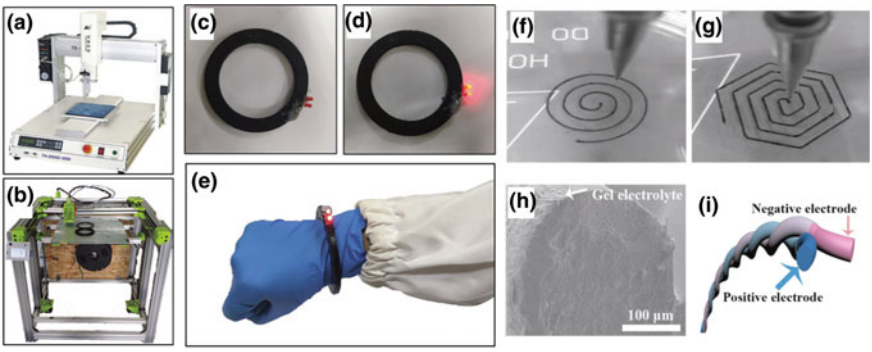

Fig. 1.18 **a** DIW 3D printer, and **b** FDM 3D printer. **c–e** Bracelet batteries with lights on and off, and bracelet battery on wrist, respectively [150]. **f**, **g** Optical images of the wet fiber during the printing process. **h** Cross-sectional SEM image of the gel electrolyte coating on the fiber. **i** Schematic of the assembled structure of the asymmetric supercapacitor [135]

by the 3D structured electrodes. An all-printed Li-ion battery was fabricated by 3D printing approaches [180]. Versatilely designed batteries can be fabricated owing to the flexibility of 3D printing. This work used well-established and commercially accepted $LiNi_{0.8}Co_{0.15}Al_{0.05}O_2$ (NCA) and natural graphite as the cathode and anode active materials, respectively, and the ink was modified to possess similar properties with slurries used in commercial coating fabrications. These make the fabrication procedure easily acceptable by industry. By integrating these 3D-printed batteries with other wearable electronics, a compact wearable system with a reduced size and weight can be developed.

Electrochemical supercapacitors have been widely used in powering wearable electronics due to their high power density, large capacity, low cost, and excellent reversibility. But the energy density is low, which impedes their practical application in wearable systems. Furthermore, the conventional planar rigid supercapacitors are not easy to be integrated into soft wearable systems. Advanced active materials can provide higher energy density and flexible configurations may make them fit for wearable applications. A fiber-shaped asymmetric supercapacitor was fabricated by 3D-printed single-walled CNT/V_2O_5 fiber cathodes and single-walled CNT/VN fiber anodes [135]. Electrodes are 3D-printed fibers, as shown in Fig. 1.18f, g. PVA/KOH gel electrolyte was printed on the surface of the as-printed positive and negative fibers (Fig. 1.18h). The two fiber-shaped electrodes are twisted to form a complete device, as shown in Fig. 1.18i. This asymmetric supercapacitor is fully printed with a maximum operating voltage of 1.6 V.

1.4.2.2 Energy Harvesting Systems

Energy harvesting technologies provide promising solutions to overcome the short lifetime of wearable energy storage devices. Unlike the batteries and supercapacitors, the energy harvesting devices do not need to charge repeatedly for continuous use. Typical energy harvesting devices can be categorized into the thermoelectric generator, oscillator, electromagnetic, piezoelectric triboelectric generators based on movement, and energy harvesting devices base on light [181]. Among them, thermoelectric generators and movement-enabled harvesting approaches are widely used in the wearable electronic system due to the capability to transfer body heat and body movement to electricity. Some remarkable works have been done in miniaturizing energy harvesting devices to supply wearable devices [182, 183]. Advanced fabrication strategies for these devices have also been investigated to reduce the manufacturing effort and cost.

An ultra-flexible 3D triboelectric generator was developed using a hybrid 3D printing technique with ink extrusion and UV curing [30]. The electrification layer is a printed UV curable composite resin structure, and the electrode is an ionic hydrogel, as shown in Fig. 1.19a. The triboelectric generator can achieve a peak power density of 10.98 W/m^3 and a transferred charge density of 0.65 mC/m^3 when working under a 1.3 Hz frequency. A self-powered buzzing SOS device was developed including printed ultra-flexible 3D triboelectric generators and external management circuits,

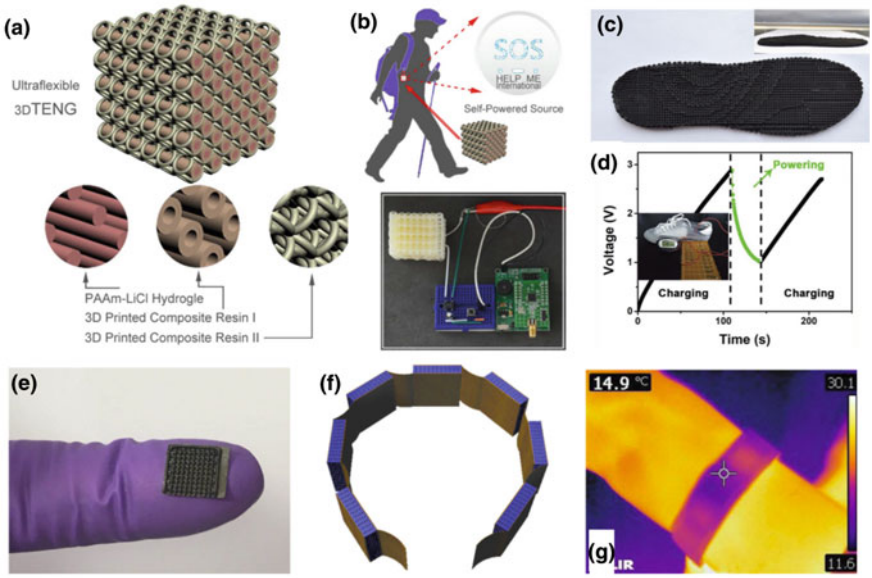

Fig. 1.19 **a** The design of an ultra-flexible 3D-printed triboelectric generator. **b** Schematic of an application as self-powered source for SOS distress signal system (top) and the picture of self-powered buzzing SOS distress system circuit (bottom) [30]. **c** Top-view images of 3D-printed triboelectric generator insole. **d** Voltage profile of a 22 μF capacitor being charged by the 3D-printed triboelectric generator insole and powering the electronic watch [137]. **e** 3D-printed flexible thermoelectric generator without the top electrode. **f** Schematic diagram of the thermoelectric generator connected in series. **g** Thermal infrared spectrum of the wristband wearable thermoelectric generator [184]

LEDs, and buzzers, as shown in Fig. 1.19b. It was also demonstrated that the triboelectric generators can be integrated with shoes to drive or charge low-power consuming electronics.

Another triboelectric generator with a tailorable sophisticated 3D architecture was fabricated using a one-step 3D printing process without additional assembling processes [137]. In this work, the electricity is generated by the compressive deformation of the scaffold electrodes consisting of CNTs and PGS. The exposed CNTs touch PGS on other filaments and become positively charged, while the PGS is negatively charged. The 3D-printed scaffold structure provides lots of open pores between the filaments, and these pores deformed/recover when the device is deformed by an external force, which will provide additional electricity due to the increase/decrease in the contact surface area. The hierarchical porous structure enabled by 3D printing results in a peak output voltage of 71 V at a 70% compression strain. A 3D-printed porous insole was fabricated and used to charge and drive electronics, as shown in Fig. 1.19c, d. And a ring-shaped triboelectric generator integrated with a LED indicator was mounted on the finger joint to monitor the finger motion. The hierarchical porous structure plays a critical role in the enhancement of performance of

this type of triboelectric generator, however, is very hard to be fabricated by conventional manufacturing approaches. 3D printing technique shows great advantage in fabricating porous or scaffold structures for advanced triboelectric generators.

Wearable thermoelectric generators are also promising for energy harvesting, which can convert body heat into electricity with conformal contact with the human body. They play an active role in wearable electronic systems to provide continuous power for small and low-power devices. Zeng et al. fabricated a flexible grid-structure-type thermoelectric generator by 3D printing, as shown in Fig. 1.19e [184]. Several generator units are further connected electrically in series and incorporated into a wristband, as shown in Fig. 1.19f, g. One side of the device is attached to the wrist skin and the other side is exposed to the air. The temperature difference between the skin and the air is converted into electric energy. The generators on the wristband can generate an output voltage and output power of 1.47 mV and 0.88 μW, respectively. The porous grid structure enabled by 3D printing can act as a thermal blocker with a low thermal conductivity and minimize unnecessary thermal energy loss.

1.4.3 Interconnects for Wearable Systems

Stretchable interconnects are one of the most important passive components in wearable electronic systems, transmitting signals between other device components. For a wearable system, the interconnects should be flexible, stretchable, and conformable to nonplanar surfaces for reliable signal transmission. Stretchable conductors that exhibit nearly constant electrical properties when undergoing large deformation and repeated loading cycles can be excellent interconnects in soft wearable systems. To achieve high stretchability with stable electrical properties, strategies employing stretchable materials s and/or stretchable structures can be used. For the stretchable material strategy, soft polymers such as TPU, silicone, PVA are widely used as the matrix materials for the interconnects, with conductive fillers added as the conducting agents. For stretchable structure strategy, the conductors are patterned into stretchable structures such as serpentine, fractal pattern, helix, and wavy structure to reduce the local stresses in the conductors. 3D printing techniques enable the printing of advanced conducting materials such as NPs, NWs, nanotubes, and graphene. For complex stretchable structures, 3D printing can also be used for fast and precise fabrication. Furthermore, due to the increasing interests in vertically configured electronics to minimize the space for wearable devices and/or achieve more functions, vertical interconnects (so-called VIAs) are required to connect between layers. 3D printing provides reliable solution to fabricate VIAs, which cannot be fabricated by conventional 2D manufacturing methods [87].

As a popular intrinsic stretchable conductive filler, liquid metal is widely used as interconnects in wearable electronic systems. 3D printing of liquid metal renders

unique advantages in fabricating sophisticated structures. A bridge structure of 3D-printed liquid metal enabled by fast oxidation of the liquid metal surface after extrusion can produce a freestanding conductive path that hangs over a previously printed line without touching it, as shown in Fig. 1.20a [45]. This makes the design of printed circuits more flexible and versatile. This method was used to fabricate a soft LED array with both transverse and longitudinal interconnects connected individually on the same plane, but no short circuit occurred between them, as shown in Fig. 1.20b. A dynamic switch circuit for LEDs enabled by the self-standing liquid metal and a reconfigurable antenna was also demonstrated, as shown in Fig. 1.20c, d. A similar strategy was reported by Park et al., with CNTs in the liquid metal to enhance the mechanical properties of the printed traces [44].

Proper structural design of the interconnects can increase the stretchability and decrease the strain sensitivity of the interconnects. A freestanding stretchable electrode based on the wavy shape was fabricated using a DIW 3D printing method [47]

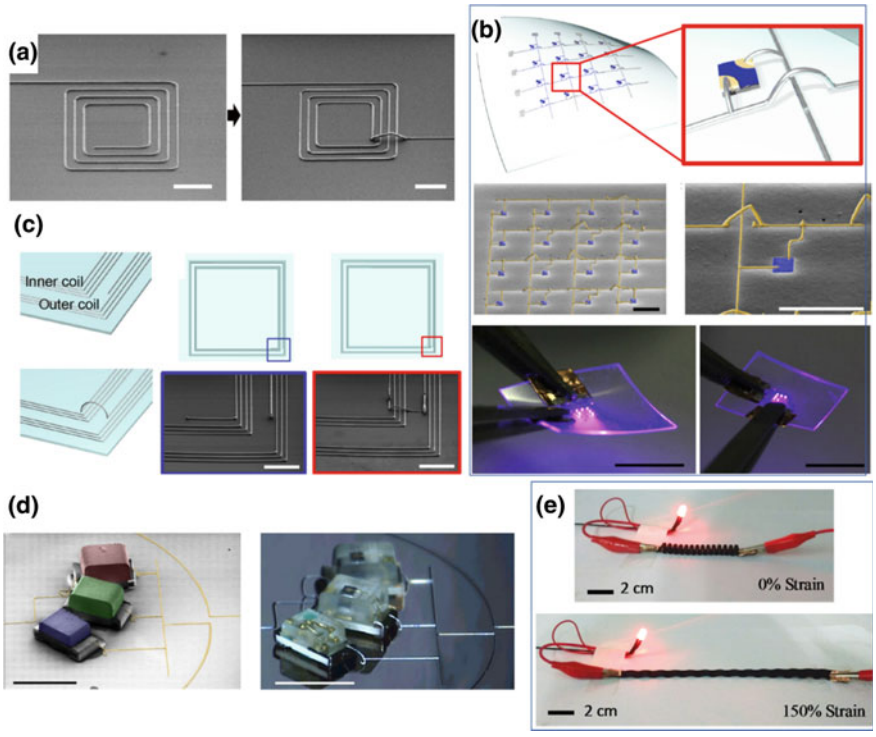

Fig. 1.20 **a** SEM images of the bridge-structured interconnects fabricated by 3D printing. Scale bars 200 mm. **b** An LED array with 3D liquid metal interconnects. **c** Schematic illustrations and SEM images of the reconfigurable antenna. **d** Colorized SEM image of three LED pixels and liquid meal interconnects, scale bar 1 mm (left) and photograph of the interconnects and LED, scale bar 1 mm (right) [45]. **e** An LED connected to the 3D-printed wavy shape interconnects under 0 (top) and 150% strain (bottom) [47]

The stretchability of the printed structure can be as high as over 300% for PDMS; and only <5% resistance change was observed at 100% strain. The 3D wavy structure was used to connect an LED light with a 12 V voltage applied, as shown in Fig. 1.20e. When the interconnect was stretched from 0 to 150%, the LED maintained a constant brightness (Table 1.2).

Table 1.2 Summary of 3D-printed wearable devices

Application	Material	Printing technique	Performance	Referecne
Capacitive strain/pressure sensor	PAAm–PEGDA hydrogel	DLP	GF: 0.92 Limit of detection: < 1.5% Strain range: 100% Stability: > 5000 cycles between 0–25% strain	[162]
Resistive strain sensor	PDMS/CNT fiber	DIW	Maximum GF: 2.5 × 10^6 at 90 to 150% strain Strain range: 150%	[185]
Strain sensor, Pressure sensor	Elastomer/carbon grease	coaxial extrusion	Strain sensor: GF of 11.8 for the strain less than 20% and 4.3 within the strain range of 20–80%, Stability of more than 10,000 cycles Pressure sensor: sensitivity of 0.562 kPa^{-1}, a response and relaxation speed of 230 ms	[177]
Resistive strain sensor	agar/calcium alginate (CA)/ PAAm hydrogel	UV curing + DIW	GF: 3.83	[164]
Capacitive pressure sensor, Resistive strain sensor	TPU/Silver flakes	DIW	Pressure sensor: elastic modulus of E ≈ 2.3 MPa; linear range of <3 MPa Strain sensor: GF of 13.3	[86]
Resistive strain sensor	PDMS/PAAm-LiCl hydrogel	UV curing + DIW	GF: 0.84 Linear range: 40%	[31]
Pressure sensor based on TENG	covalent crosslinked elastomer/CNT/AgNF/CB	DIW	Sensitivity: 0.147–0.528 MPa^{-1} Stability: 1.3% mass loss in 20 days	[171]
Resistive tactile sensors	AgNPs/silicone, AgNW/ silicone, Silicone, Pluronic	DIW	GF: 180 Stability: more than 100 cycles	[72]

(continued)

Table 1.2 (continued)

Application	Material	Printing technique	Performance	Referecne
Piezoresistive pressure sensor	PDMS, TPU/CB/NaCl , TPU/Ag microflakes	DIW	Sensitivity: 5.54 kPa^{-1} for <10 kPa, 0.123 kPa^{-1} for 10–100 kPa and 0.0048 kPa^{-1} for 100–800 kPa GF: 13.3 Stability: more than 10,000 cycles	[73]
Piezoresistive pressure sensor	Modified PUAs	DLP	Sensitivity: 2010.1 MPa^{-1} in the region of 0.09−0.23 MPa Stability: After 100 compression cycles at 80% strain, the maximum compressive stress remained above 93.3%	[37]
Piezoresistive pressure sensor	CNTs/silica NPs (SiNPs)/Ecoflex	DIW	Sensitivity: 0.096 kPa^{-1} Range: 0−175 kPa Stability: over 10,000 compression cycles	[68]
Piezoelectric air pressure sensor	Functionalized piezoelectric particles	SLA	Detectable low aire pressure: <50 Pa	[70]
Temperature sensor	Graphene/PDMS	DIW	Resolution: 0.5 °C Sensitivity: 0.008 $°C^{-1}$ Response time: 1.32−3.91 s Recovery time: 1.01−4.58 s	[178]
Photodetector	P3HT:PCBM, liquid metal, silicone, PEDOT:PSS, AgNPs	DIW	External quantum efficiency: 25.3%,	[156]
TENG	acrylate oligomer-based UV curable polymer, PAAm-LiCl hydrogel	UV curing + DIW	Power density: 10.98 W/m3 under a frequency of 1.3 Hz, Transferred charge density: 0.65 mC/m^{-2} under a frequency of 1.3 Hz,	[30]

(continued)

Table 1.2 (continued)

Application	Material	Printing technique	Performance	Referecne
TENG	PUA/silver flakes/liquid metal	DIW	Stretchability: 2500% power density: 40 μWcm^{-2} with load resistance of 1MΩ	[32]
TENG	poly(glycerol sebacate)/(CNTs)	DIW	Power density: 1.11 W m^{-3} Stability: more than 6000 cycles at a compression strain of 40%	[137]
Lithium-Sulfur Battery	GO/phenolformaldehyde (PF)/SiO_2	FDM	Specific capacity: 505.4 mAh g^{-1} after 500 cycles Active material loading: 10.2 mg cm^{-1}	[150]
Interconnect	PDMS/CNT composite	DIW	Stretchability: 315% Resistance change: 5% change at 100% strain and 35% change at 200% Stability: >120 cycles between 0–100% strain	[47]
Interconnect	Liquide metal	DIW	Minimum line width: 1.9 mm 60–90 Ω contact resistance between interconnect and Ag, Au, and Cu	[45]
Interconnect	TPU/AgNW	FDM	System Stretchability: 440% Interconnect stretchability: 25 000% Stability: over 1000 cycles under Interconnect stretchability	[67]

1.5 Summary and Outlook

As an advanced additive manufacturing approach, 3D printing has been applied to a wide variety of applications. Soft wearable electronics are thriving with the advances in functional materials and new fabrication approaches such as 3D printing. This chapter has provided a systematic perspective on the 3D printing techniques, 3D printable materials, and wearable electronic devices enabled by the 3D printing

techniques. In our opinion, the following directions are promising in order to expand the applications of 3D printing in wearable electronics:

1. Investigating advanced ink formulation for printing more functional materials. More and more emerging nanomaterials are used to fabricate wearable electronics. Although a variety of widely used materials discussed in this chapter, e.g., nanoparticles, carbon-based nanomaterials, and liquid metal, have been proven to be printable using a 3D printing platform, the conducting fillers in the inks are still limited by the strict requirements on the thermal properties for FDM-based printing and rheology properties for DIW-based printing.
2. Developing and optimizing 3D printing systems that are applicable to multiple materials and structures. Using one platform to prepare different components in one device, i.e., all-printed devices, can further simplify the manufacturing procedure and lower the cost. This requires the 3D printer to be capable of printing inks with different properties into a variety of different structures. For instance, it should be compatible with structural materials like polymers and functional materials like metal NPs/NWs. It should be able to construct different types of structures such as in-pane traces, vertical structures, grid structures, and self-standing bridges.
3. Further increasing the resolution of the printed features. Minimizing the footprint and increasing the integration level of wearable devices are of great significance in practical applications. However, to date, most of the widely used 3D printing techniques such as SLA, DLP, and FDM have much lower resolution compared to conventional lithography manufacturing approaches.
4. Improving printing capabilities by incorporating advanced algorithms to control the 3D printer, such as predictive algorithms to anticipate future deformations and motions.

References

1. Trung TQ, Lee NE (2016) Flexible and stretchable physical sensor integrated platforms for wearable human-activity monitoringand personal healthcare. Adv Mater 28(22):4338–4372
2. Ma Y, Zhang Y, Cai S, Han Z, Liu X, Wang F et al (2019) Flexible hybrid electronics for digital healthcare. Adv Mater e1902062
3. Yao S, Yang J, Poblete FR, Hu X, Zhu Y (2019) Multifunctional electronic textiles using silver nanowire composites. ACS Appl Mater Interfaces 11(34):31028–31037
4. Yao S, Myers A, Malhotra A, Lin F, Bozkurt A, Muth JF et al (2017) A Wearable hydration sensor with conformal nanowire electrodes. Adv Healthc Mater 6(6):1601159
5. Yao S, Swetha P, Zhu Y (2018) Nanomaterial-enabled wearable sensors for healthcare. Adv Healthc Mater 7(1):1700889
6. Liu Y, Shukla D, Newman H, Zhu Y (2021) Soft wearable sensors for monitoring symptoms of COVID-19 and other respiratory diseases: a review. Progress Biomed Eng 4(1):012001
7. Lee H, Song C, Hong YS, Kim MS, Cho HR, Kang T et al (2017) Wearable/disposable sweat-based glucose monitoring device with multistage transdermal drug delivery module. Sci Adv 3(3):1601314

8. Wu S, Cui Z, Baker GL, Mahendran S, Xie Z, Zhu Y (2021) A biaxially stretchable and self-sensing textile heater using silver nanowire composite. ACS Appl Mater Interfaces 13(49):59085–59091
9. Soto F, Mishra RK, Chrostowski R, Martin A, Wang J (2017) Epidermal tattoo patch for ultrasound-based transdermal microballistic delivery. Adv Mater Technol 2(12):1700210
10. Amjadi M, Sheykhansari S, Nelson BJ, Sitti M (2018) Recent advances in wearable transdermal delivery systems. Adv Mater 30(7):1704530
11. Kim J, Shim HJ, Yang J, Choi MK, Kim DC, Kim J et al (2017) Ultrathin quantum dot display integrated with wearable electronics. Adv Mater 29(38):1700217
12. Zhang T, Li Z, Li K, Yang X (2019) Flexible pressure sensors with wide linearity range and high sensitivity based on selective laser sintering 3D printing. Adv Mater Technol 4(12):1900679
13. Li Z, Liu Y, Hossain O, Paul R, Yao S, Wu S et al (2021) Real-time monitoring of plant stresses via chemiresistive profiling of leaf volatiles by a wearable sensor. Matter 4(7):2553–2570
14. Zhou W, Yao S, Wang H, Du Q, Ma Y, Zhu Y (2020) Gas-permeable, ultrathin, stretchable epidermal electronics with porous electrodes. ACS Nano 14(5):5798–5805
15. Liu Y, Wang H, Zhu Y (2021) Recycling of nanowire percolation network for sustainable soft electronics. Adv Electron Mater 7(9):2100588
16. Xue Z, Song H, Rogers JA, Zhang Y, Huang Y (2019) Mechanically-guided structural designs in stretchable inorganic electronics. Adv Mater e1902254
17. Zhang Y, Xu S, Fu H, Lee J, Su J, Hwang KC et al (2013) Buckling in serpentine microstructures and applications in elastomer-supported ultra-stretchable electronics with high areal coverage. Soft Matter 9(33):8062–8070
18. Chang JK, Chang HP, Guo Q, Koo J, Wu CI, Rogers JA (2018) Biodegradable electronic systems in 3D, heterogeneously integrated formats. Adv Mater 30(11):1704955
19. Pan T, Pharr M, Ma Y, Ning R, Yan Z, Xu R et al (2017) Experimental and theoretical studies of serpentine interconnects on ultrathin elastomers for stretchable electronics. Adv Func Mater 27(37):1702589
20. Hong YJ, Jeong H, Cho KW, Lu N, Kim DH (2019) Wearable and implantable devices for cardiovascular healthcare: from monitoring to therapy based on flexible and stretchable electronics. Adv Func Mater 29(19):1808247
21. Huang Z, Hao Y, Li Y, Hu H, Wang C, Nomoto A et al (2018) Three-dimensional integrated stretchable electronics. Nat Electron 1(8):473–480
22. Koo JH, Jeong S, Shim HJ, Son D, Kim J, Kim DC et al (2017) Wearable electrocardiogram monitor using carbon nanotube electronics and color-tunable organic light-emitting diodes. ACS Nano 11(10):10032–10041
23. Park M, Do K, Kim J, Son D, Koo JH, Park J et al (2015) Oxide nanomembrane hybrids with enhanced mechano- and thermo-sensitivity for semitransparent epidermal electronics. Adv Healthcare Mater 4(7):992–997
24. Zou Z, Zhu C, Li Y, Lei X, Zhang W, Xiao J (2018) Rehealable, fully recyclable, and malleable electronic skin enabled by dynamic covalent thermoset nanocomposite. Sci Adv 4(2):eaaq0508
25. Huang Q, Zhu Y (2019) Printing conductive nanomaterials for flexible and stretchable electronics: a review of materials, processes, and applications. Adv Mater Technol 4(5):1800546
26. Cui Z, Han Y, Huang Q, Dong J, Zhu Y (2018) Electrohydrodynamic printing of silver nanowires for flexible and stretchable electronics. Nanoscale 10(15):6806–6811
27. Huang Q, Zhu Y (2018) Gravure printing of water-based silver nanowire ink on plastic substrate for flexible electronics. Sci Rep 8(1):15167
28. Huang Q, Zhu Y (2021) Patterning of metal nanowire networks: methods and applications. ACS Appl Mater Interfaces 13(51):60736–60762
29. Tan LJ, Zhu W, Zhou K (2020) Recent progress on polymer materials for additive manufacturing. Adv Func Mater 30(43):2003062
30. Chen B, Tang W, Jiang T, Zhu L, Chen X, He C et al (2018) Three-dimensional ultraflexible triboelectric nanogenerator made by 3D printing. Nano Energy 45:380–389

31. Tian K, Bae J, Bakarich SE, Yang C, Gately RD, Spinks GM et al (2017) 3D printing of transparent and conductive heterogeneous hydrogel-elastomer systems. Adv Mater 29(10):1604827
32. Parida K, Thangavel G, Cai G, Zhou X, Park S, Xiong J et al (2019) Extremely stretchable and self-healing conductor based on thermoplastic elastomer for all-three-dimensional printed triboelectric nanogenerator. Nat Commun 10(1):2158
33. Emon MOF, Alkadi F, Philip DG, Kim D-H, Lee K-C, Choi J-W (2019) Multi-material 3D printing of a soft pressure sensor. Addit Manuf 28:629–638
34. Odent J, Wallin TJ, Pan WY, Kruemplestaedter K, Shepherd RF, Giannelis EP (2017) Highly elastic, transparent, and conductive 3d-printed ionic composite hydrogels. Adv Func Mater 27(33):1701807
35. Ambrosi A, Pumera M (2016) 3D-printing technologies for electrochemical applications. Chem Soc Rev 45(10):2740–2755
36. Billiet T, Vandenhaute M, Schelfhout J, Van Vlierberghe S, Dubruel P (2012) A review of trends and limitations in hydrogel-rapid prototyping for tissue engineering. Biomaterials 33(26):6020–6041
37. Peng S, Li Y, Wu L, Zhong J, Weng Z, Zheng L et al (2020) 3D Printing mechanically robust and transparent polyurethane elastomers for stretchable electronic sensors. ACS Appl Mater Interfaces 12(5):6479–6488
38. Zarek M, Layani M, Cooperstein I, Sachyani E, Cohn D, Magdassi S (2016) 3D printing of shape memory polymers for flexible electronic devices. Adv Mater 28(22):4449–4454
39. Cheng-Yu H, Ahmed Abro Z, Yi-Fan Z, Ahmed LR (2019) An FBG-based smart wearable ring fabricated using FDM for monitoring body joint motion. J Ind Text 50(10):1660–1673
40. Yang W, Zhao W, Li Q, Li H, Wang Y, Li Y et al (2020) Fabrication of smart components by 3D printing and laser-scribing technologies. ACS Appl Mater Interfaces 12(3):3928–3935
41. Liang K, Carmone S, Brambilla D, Leroux JC (2018) 3D printing of a wearable personalized oral delivery device: a first-in-human study. Sci Adv 4(5):eaat2544
42. Li Z, Rathore AS, Song C, Wei S, Wang Y, Xu W (2018) PrinTracker: Fingerprinting 3D printers using commodity scanners. In: Proceedings of the 2018 ACM SIGSAC conference on computer and communications security, pp 1306–1323
43. Owens CE, Headrick RJ, Williams SM, Fike AJ, Pasquali M, McKinley GH et al (2021) Substrate-versatile direct-write printing of carbon nanotube-based flexible conductors, circuits, and sensors. Adv Func Mater 31(25):2100245
44. Park YG, Min H, Kim H, Zhexembekova A, Lee CY, Park JU (2019) Three-dimensional, high-resolution printing of carbon nanotube/liquid metal composites with mechanical and electrical reinforcement. Nano Lett 19(8):4866–4872
45. Park YG, An HS, Kim JY, Park JU (2019) High-resolution, reconfigurable printing of liquid metals with three-dimensional structures. Sci Adv 5(6):eaaw2844
46. Zhang Y, Shi G, Qin J, Lowe SE, Zhang S, Zhao H et al (2019) Recent progress of direct ink writing of electronic components for advanced wearable devices. ACS Appl Electron Mater 1(9):1718–1734
47. Wei H, Li K, Liu WG, Meng H, Zhang PX, Yan CY (2017) 3D Printing of free-standing stretchable electrodes with tunable structure and stretchability. Adv Eng Mater 19(11):1700341
48. Li H, Tan YJ, Leong KF, Li L (2017) 3D Bioprinting of highly thixotropic alginate/methylcellulose hydrogel with strong interface bonding. ACS Appl Mater Interfaces 9(23):20086–20097
49. Zacharatos F, Theodorakos I, Karvounis P, Tuohy S, Braz N, Melamed S et al (2018) Selective laser sintering of laser printed Ag nanoparticle micropatterns at high repetition rates. Materials (Basel). 11(11):2142
50. Wang J, Sun S, Li X, Fei G, Wang Z, Xia H (2021) Selective laser sintering of polydimethylsiloxane composites. 3D Printing Addit Manuf
51. Ronca A, Rollo G, Cerruti P, Fei G, Gan X, Buonocore G et al (2019) Selective laser sintering fabricated thermoplastic polyurethane/graphene cellular structures with tailorable properties and high strain sensitivity. Appl Sci 9(5):864

52. Li Z, Wang Z, Gan X, Fu D, Fei G, Xia H (2017) Selective laser sintering 3D printing: a way to construct 3D electrically conductive segregated network in polymer matrix. Macromol Mater Eng 302(11):1700211
53. Agarwala S, Goh GL, Le Dinh TS, An J, Peh ZK, Yeong WY et al (2019) Wearable bandage-based strain sensor for home healthcare: combining 3D aerosol jet printing and laser sintering. ACS Sens 4(1):218–226
54. Choi S, Lee H, Ghaffari R, Hyeon T, Kim DH (2016) Recent advances in flexible and stretchable bio-electronic devices integrated with nanomaterials. Adv Mater 28(22):4203–4218
55. Park S, Kim H, Vosgueritchian M, Cheon S, Kim H, Koo JH et al (2014) Stretchable energy-harvesting tactile electronic skin capable of differentiating multiple mechanical stimuli modes. Adv Mater 26(43):7324–7332
56. Irimia-Vladu M (2014) "Green" electronics: biodegradable and biocompatible materials and devices for sustainable future. Chem Soc Rev 43(2):588–610
57. Ganesh RS, Yoon HJ, Kim SW (2020) Recent trends of biocompatible triboelectric nanogenerators toward self-powered e-skin. EcoMat. 2(4):12065
58. Lee HR, Kim CC, Sun JY (2018) Stretchable Ionics—a promising candidate for upcoming wearable devices. Adv Mater 30(42):e1704403
59. Song Y, Min J, Gao W (2019) Wearable and implantable electronics: moving toward precision therapy. ACS Nano 13(11):12280–12286
60. Choi S, Han SI, Jung D, Hwang HJ, Lim C, Bae S et al (2018) Highly conductive, stretchable and biocompatible Ag–Au core-sheath nanowire composite for wearable and implantable bioelectronics. Nat Nanotechnol 13(11):1048–1056
61. Sekitani T, Yokota T, Kuribara K, Kaltenbrunner M, Fukushima T, Inoue Y et al (2016) Ultraflexible organic amplifier with biocompatible gel electrodes. Nat Commun 7:11425
62. Wang C, Yokota T, Someya T (2021) Natural biopolymer-based biocompatible conductors for stretchable bioelectronics. Chem Rev 121(4):2109–2146
63. Oh JY, Bao Z (2019) Second skin enabled by advanced electronics. Adv Sci (Weinh) 6(11):1900186
64. Wei H, Cauchy X, Navas IO, Abderrafai Y, Chizari K, Sundararaj U et al (2019) Direct 3D printing of hybrid nanofiber-based nanocomposites for highly conductive and shape memory applications. ACS Appl Mater Interfaces 11(27):24523–24532
65. Chen Z, Zhao D, Liu B, Nian G, Li X, Yin J et al (2019) 3D printing of multifunctional hydrogels. Adv Func Mater 29(20):1900971
66. Lei ZY, Wang QK, Wu PY (2017) A multifunctional skin-like sensor based on a 3D printed thermo-responsive hydrogel. Mater Horiz 4(4):694–700
67. Jo M, Bae S, Oh I, Jeong JH, Kang B, Hwang SJ et al (2019) 3D Printer-based encapsulated origami electronics for extreme system stretchability and high areal coverage. ACS Nano 13(11):12500–12510
68. Tang Z, Jia S, Zhou C, Li B (2020) 3D printing of highly sensitive and large-measurement-range flexible pressure sensors with a positive piezoresistive effect. ACS Appl Mater Interfaces 12(25):28669–28680
69. Huang K, Dong S, Yang J, Yan J, Xue Y, You X et al (2019) Three-dimensional printing of a tunable graphene-based elastomer for strain sensors with ultrahigh sensitivity. Carbon 143:63–72
70. Yao D, Cui H, Hensleigh R, Smith P, Alford S, Bernero D et al (2019) Achieving the upper bound of piezoelectric response in tunable, wearable 3D printed nanocomposites. advanced functional materials 29(42)
71. Zhou LY, Gao Q, Zhan JF, Xie CQ, Fu JZ, He Y (2018) Three-dimensional printed wearable sensors with liquid metals for detecting the pose of snakelike soft robots. ACS Appl Mater Interfaces 10(27):23208–23217
72. Guo SZ, Qiu K, Meng F, Park SH, McAlpine MC (2017) 3D printed stretchable tactile sensors. Adv Mater 29(27):1701218
73. Wang Z, Guan X, Huang H, Wang H, Lin W, Peng Z (2019) Full 3D printing of stretchable piezoresistive sensor with hierarchical porosity and multimodulus architecture. Adv Func Mater 29(11):1807569

74. Wong J, Gong AT, Defnet PA, Meabe L, Beauchamp B, Sweet RM et al (2019) 3D Printing Ionogel auxetic frameworks for stretchable sensors. Adv Mater Technol 4(9):1900452
75. Yao S, Ren P, Song R, Liu Y, Huang Q, Dong J et al (2020) Nanomaterial-enabled flexible and stretchable sensing systems: processing, integration, and applications. Adv Mater 32(15):e1902343
76. Yao S, Zhu Y (2015) Nanomaterial-enabled stretchable conductors: strategies, materials and devices. Adv Mater 27(9):1480–1511
77. Jayathilaka W, Qi K, Qin Y, Chinnappan A, Serrano-Garcia W, Baskar C et al (2019) Significance of nanomaterials in wearables: a review on wearable actuators and sensors. Adv Mater 31(7):e1805921
78. Son D, Bao Z (2018) Nanomaterials in skin-inspired electronics: toward soft and robust skin-like electronic nanosystems. ACS Nano 12(12):11731–11739
79. Kamyshny A, Magdassi S (2019) Conductive nanomaterials for 2D and 3D printed flexible electronics. Chem Soc Rev 48(6):1712–1740
80. Cui Z, Poblete FR, Cheng G, Yao S, Jiang X, Zhu Y (2014) Design and operation of silver nanowire based flexible and stretchable touch sensors. J Mater Res 30(1):79–85
81. Zhang S, Cai L, Li W, Miao J, Wang T, Yeom J et al (2017) Fully printed silver-nanoparticle-based strain gauges with record high sensitivity. Adv Electron Mater 3(7):1700067
82. Serway RA, Jewett JW (2018) Physics for scientists and engineers. Cengage learning
83. Gaspar C, Passoja S, Olkkonen J, Smolander M (2016) IR-sintering efficiency on inkjet-printed conductive structures on paper substrates. Microelectron Eng 149:135–140
84. Lee HH, Chou KS, Huang KC (2005) Inkjet printing of nanosized silver colloids. Nanotechnology 16(10):2436–2441
85. Cui Z, Poblete FR, Zhu Y (2019) Tailoring the temperature coefficient of resistance of silver nanowire nanocomposites and their application as stretchable temperature sensors. ACS Appl Mater Interfaces 11(19):17836–17842
86. Valentine AD, Busbee TA, Boley JW, Raney JR, Chortos A, Kotikian A et al (2017) Hybrid 3D printing of soft electronics. Adv Mater 29(40):1703817
87. Sowade E, Polomoshnov M, Willert A, Baumann RR (2019) Toward 3D-printed electronics: inkjet-printed vertical metal wire interconnects and screen-printed batteries. Adv Eng Mater 21(10):1900568
88. Yu Z, Zhang Q, Li L, Chen Q, Niu X, Liu J et al (2011) Highly flexible silver nanowire electrodes for shape-memory polymer light-emitting diodes. Adv Mater 23(5):664–668
89. Lee P, Lee J, Lee H, Yeo J, Hong S, Nam KH et al (2012) Highly stretchable and highly conductive metal electrode by very long metal nanowire percolation network. Adv Mater 24(25):3326–3332
90. Jiang ZH, Cui Z, Yue T, Zhu Y, Werner DH (2017) Compact, highly efficient, and fully flexible circularly polarized antenna enabled by silver nanowires for wireless body-area networks. IEEE Trans Biomed Circ Syst 11(4):920–932
91. Zhu B, Ling Y, Yap LW, Yang M, Lin F, Gong S et al (2019) Hierarchically structured vertical gold nanowire array-based wearable pressure sensors for wireless health monitoring. ACS Appl Mater Interfaces 11(32):29014–29021
92. Han S, Kim MK, Wang B, Wie DS, Wang S, Lee CH (2016) Mechanically reinforced skin-electronics with networked nanocomposite elastomer. Adv Mater 28(46):10257–10265
93. Liang J, Li L, Tong K, Ren Z, Hu W, Niu X et al (2014) Silver nanowire percolation network soldered with graphene oxide at room temperature and its application for fully stretchable polymer light-emitting diodes. ACS Nano 8(2):1590–1600
94. Xu F, Zhu Y (2012) Highly conductive and stretchable silver nanowire conductors. Adv Mater 24(37):5117–5122
95. Song L, Myers AC, Adams JJ, Zhu Y (2014) Stretchable and reversibly deformable radio frequency antennas based on silver nanowires. ACS Appl Mater Interfaces 6(6):4248–4253
96. Yao S, Cui J, Cui Z, Zhu Y (2017) Soft electrothermal actuators using silver nanowire heaters. Nanoscale 9(11):3797–3805

97. Yan P, Brown E, Su Q, Li J, Wang J, Xu C et al (2017) 3D printing hierarchical silver nanowire aerogel with highly compressive resilience and tensile elongation through tunable poisson's ratio. Small 13(38):1701756
98. Liu S, Shi X, Li X, Sun Y, Zhu J, Pei Q et al (2018) A general gelation strategy for 1D nanowires: dynamically stable functional gels for 3D printing flexible electronics. Nanoscale 10(43):20096–20107
99. Han Y, Dong J (2018) Electrohydrodynamic (EHD) printing of molten metal ink for flexible and stretchable conductor with self-healing capability. Adv Mater Technol 3(3):1700268
100. Neumann TV, Dickey MD (2020) Liquid metal direct write and 3D printing: a review. Adv Mater Technol 2000070
101. Han Y, Dong J (2017) High-resolution direct printing of molten-metal using electrohydrodynamic jet plotting. Manufact Lett 12:6–9
102. Kang L, Chen H, Yang Z-J, Yuan Y, Huang H, Yang B et al (2018) Seesaw-like polarized transmission behavior of silver nanowire arrays aligned by off-center spin-coating. J Appl Phys 123(20):205110
103. Ladd C, So JH, Muth J, Dickey MD (2013) 3D printing of free standing liquid metal microstructures. Adv Mater 25(36):5081–5085
104. Lipomi DJ, Vosgueritchian M, Tee BC, Hellstrom SL, Lee JA, Fox CH et al (2011) Skin-like pressure and strain sensors based on transparent elastic films of carbon nanotubes. Nat Nanotechnol 6(12):788–792
105. Li Y, Zhu H, Wang Y, Ray U, Zhu S, Dai J et al (2017) Cellulose-Nanofiber-enabled 3D printing of a carbon-nanotube microfiber network. Small Methods 1(10):1700222
106. Yamada T, Hayamizu Y, Yamamoto Y, Yomogida Y, Izadi-Najafabadi A, Futaba DN et al (2011) A stretchable carbon nanotube strain sensor for human-motion detection. Nat Nanotechnol 6(5):296–301
107. Dorozhkin PS, Tovstonog SV, Golberg D, Zhan J, Ishikawa Y, Shiozawa M et al (2005) A liquid-Ga-filled carbon nanotube: a miniaturized temperature sensor and electrical switch. Small 1(11):1088–1093
108. Wang K, Chang Y-H, Zhang C, Wang B (2016) Conductive-on-demand: tailorable polyimide/carbon nanotube nanocomposite thin film by dual-material aerosol jet printing. Carbon 98:397–403
109. Goh GL, Agarwala S, Yeong WY (2019) Aerosol-jet-printed preferentially aligned carbon nanotube twin-lines for printed electronics. ACS Appl Mater Interfaces 11(46):43719–43730
110. Sun S, Guo L, Chang X, Liu Y, Niu S, Lei Y et al (2019) A wearable strain sensor based on the ZnO/graphene nanoplatelets nanocomposite with large linear working range. J Mater Sci 54(9):7048–7061
111. Trung TQ, Ramasundaram S, Hong SW, Lee N-E (2014) Flexible and transparent nanocomposite of reduced graphene oxide and P(VDF-TrFE) copolymer for high thermal responsivity in a field-effect transistor. Adv Func Mater 24(22):3438–3445
112. Wei Y, Qiao Y, Jiang G, Wang Y, Wang F, Li M et al (2019) A Wearable skinlike ultra-sensitive artificial graphene throat. ACS Nano 13(8):8639–8647
113. Kabiri Ameri S, Ho R, Jang H, Tao L, Wang Y, Wang L et al (2017) Graphene electronic tattoo sensors. ACS Nano 11(8):7634–7641
114. Yan C, Wang J, Lee PS (2015) Stretchable graphene thermistor with tunable thermal index. ACS Nano 9(2):2130–2137
115. Zhu YS, Li JW, Cai HB, Wua YM, Ding HY, Pan N et al (2018) Highly sensitive and skin-like pressure sensor based on asymmetric double-layered structures of reduced graphite oxide. Sens Actuators B-Chem 255:1262–1267
116. Jason NN, Wang SJ, Bhanushali S, Cheng W (2016) Skin inspired fractal strain sensors using a copper nanowire and graphite microflake hybrid conductive network. Nanoscale 8(37):16596–16605
117. Arduini F, Zanardi C, Cinti S, Terzi F, Moscone D, Palleschi G et al (2015) Effective electrochemical sensor based on screen-printed electrodes modified with a carbon black-Au nanoparticles composite. Sens Actuators B-Chem 212:536–543

118. Kim J, Sempionatto JR, Imani S, Hartel MC, Barfidokht A, Tang G et al (2018) Simultaneous monitoring of sweat and interstitial fluid using a single wearable biosensor platform. Adv Sci (Weinh). 5(10):1800880
119. Mohan AMV, Kim N, Gu Y, Bandodkar AJ, You JM, Kumar R et al (2017) Merging of thin- and thick-film fabrication technologies: toward soft stretchable "Island–Bridge" devices. Adv Mater Technol. 2(4):1600284
120. Salvetat JP, Briggs GAD, Bonard JM, Bacsa RR, Kulik AJ, Stockli T et al (1999) Elastic and shear moduli of single-walled carbon nanotube ropes. Phys Rev Lett 82(5):944–947
121. Yu MF, Files BS, Arepalli S, Ruoff RS (2000) Tensile loading of ropes of single wall carbon nanotubes and their mechanical properties. Phys Rev Lett 84(24):5552–5555
122. Cao Q, Yu Q, Connell DW, Yu G (2013) Titania/carbon nanotube composite (TiO_2/CNT) and its application for removal of organic pollutants. Clean Technol Environ Policy 15(6):871–880
123. Sreekumar TV, Liu T, Kumar S, Ericson LM, Hauge RH, Smalley RE (2002) Single-wall carbon nanotube films. Chem Mater 15(1):175–178
124. Slobodian P, Riha P, Lengalova A, Saha P (2010) Compressive stress-electrical conductivity characteristics of multiwall carbon nanotube networks. J Mater Sci 46(9):3186–3190
125. Lamela H, Dadrasnia E (2012) Terahertz analysis reveals nanostructural dependence of carbon thin-film properties. SPIE Newsroom
126. Dai H, Wong EW, Lieber CM (1996) Probing electrical transport in nanomaterials: conductivity of individual carbon nanotubes. Science 272(5261):523–526
127. Bachtold A, Henny M, Terrier C, Strunk C, Schönenberger C, Salvetat JP et al (1998) Contacting carbon nanotubes selectively with low-ohmic contacts for four-probe electric measurements. Appl Phys Lett 73(2):274–276
128. Xu F, Wang X, Zhu Y, Zhu Y (2012) Wavy ribbons of carbon nanotubes for stretchable conductors. Adv Func Mater 22(6):1279–1283
129. Kim JH, Lee S, Wajahat M, Jeong H, Chang WS, Jeong HJ et al (2016) Three-dimensional printing of highly conductive carbon nanotube microarchitectures with fluid ink. ACS Nano 10(9):8879–8887
130. Goh GL, Agarwala S, Yeong WY (2019) Directed and on-demand alignment of carbon nanotube: a review toward 3D printing of electronics. Adv Mater Interfaces 6(4):1801318
131. Ribeiro B, Botelho EC, Costa ML, Bandeira CF (2017) Carbon nanotube buckypaper reinforced polymer composites: a review. Polímeros 27(3):247–255
132. Zhu Y, Xu F (2012) Buckling of aligned carbon nanotubes as stretchable conductors: a new manufacturing strategy. Adv Mater 24(8):1073–1077
133. Roh E, Hwang BU, Kim D, Kim BY, Lee NE (2015) Stretchable, transparent, ultrasensitive, and patchable strain sensor for human-machine interfaces comprising a nanohybrid of carbon nanotubes and conductive elastomers. ACS Nano 9(6):6252–6261
134. Doganay D, Cicek MO, Durukan MB, Altuntas B, Agbahca E, Coskun S et al (2021) Fabric based wearable triboelectric nanogenerators for human machine interface. Nano Energy
135. Zhao J, Zhang Y, Huang Y, Xie J, Zhao X, Li C et al (2018) 3D Printing fiber electrodes for an all-fiber integrated electronic device via hybridization of an asymmetric supercapacitor and a temperature sensor. Adv Sci (Weinh) 5(11):1801114
136. Abshirini M, Charara M, Marashizadeh P, Saha MC, Altan MC, Liu Y (2019) Functional nanocomposites for 3D printing of stretchable and wearable sensors. Appl Nanosci 9(8):2071–2083
137. Chen S, Huang T, Zuo H, Qian S, Guo Y, Sun L et al (2018) A Single integrated 3D-printing process customizes elastic and sustainable triboelectric nanogenerators for wearable electronics. Adv Func Mater 28(46):1805108
138. Castro Neto AH, Guinea F, Peres NMR, Novoselov KS, Geim AK (2009) The electronic properties of graphene. Rev Mod Phys 81(1):109–162
139. Tang X, Zhou H, Cai Z, Cheng D, He P, Xie P et al (2018) Generalized 3D printing of graphene-based mixed-dimensional hybrid aerogels. ACS Nano 12(4):3502–3511
140. Wang Y, Wang L, Yang T, Li X, Zang X, Zhu M et al (2014) Wearable and highly sensitive graphene strain sensors for human motion monitoring. Adv Func Mater 24(29):4666–4670

141. Wang Y, Yang R, Shi Z, Zhang L, Shi D, Wang E et al (2011) Super-elastic graphene ripples for flexible strain sensors. ACS Nano 5(5):3645–3650
142. Wang Z, Liu X, Shen X, Han NM, Wu Y, Zheng Q et al (2018) An Ultralight graphene honeycomb sandwich for stretchable light-emitting displays. Adv Func Mater 28(19):1707043
143. Bay HH, Vo R, Dai X, Hsu HH, Mo Z, Cao S et al (2019) Hydrogel Gate graphene field-effect transistors as multiplexed biosensors. Nano Lett 19(4):2620–2626
144. Sun Q, Kim DH, Park SS, Lee NY, Zhang Y, Lee JH et al (2014) Transparent, low-power pressure sensor matrix based on coplanar-gate graphene transistors. Adv Mater 26(27):4735–4740
145. Chen X, Shehzad K, Gao L, Long M, Guo H, Qin S et al (2019) Graphene hybrid structures for integrated and flexible optoelectronics. Adv Mater e1902039
146. Choi MK, Park I, Kim DC, Joh E, Park OK, Kim J et al (2015) Thermally controlled, patterned graphene transfer printing for transparent and wearable electronic/optoelectronic system. Adv Func Mater 25(46):7109–7118
147. Bellani S, Petroni E, Del Rio Castillo AE, Curreli N, Martín-García B, Oropesa-Nuñez R et al (2019) Scalable production of graphene inks via wet-jet milling exfoliation for screen-printed micro-supercapacitors. Adv Func Mater 29(14):1807659
148. Jakus AE, Secor EB, Rutz AL, Jordan SW, Hersam MC, Shah RN (2015) Three-dimensional printing of high-content graphene scaffolds for electronic and biomedical applications. ACS Nano 9(4):4636–4648
149. Kwon SN, Kim SW, Kim IG, Hong YK, Na SI (2018) Direct 3D Printing of graphene nanoplatelet/silver nanoparticle-based nanocomposites for multiaxial piezoresistive sensor applications. Adv Mater Technol 1800500
150. Chen C, Jiang J, He W, Lei W, Hao Q, Zhang X (2020) 3D printed high-loading lithium-sulfur battery toward wearable energy storage. Adv Funct Mater 30(10)
151. Savagatrup S, Chan E, Renteria-Garcia SM, Printz AD, Zaretski AV, O'Connor TF et al (2015) Plasticization of PEDOT:PSS by common additives for mechanically robust organic solar cells and wearable sensors. Adv Func Mater 25(3):427–436
152. Nair NM, Pakkathillam JK, Kumar K, Arunachalam K, Ray D, Swaminathan P (2020) Printable silver nanowire and PEDOT:PSS nanocomposite ink for flexible transparent conducting applications. ACS Appl Electron Mater
153. Nair NM, Pakkathillam JK, Kumar K, Arunachalam K, Ray D, Swaminathan P (2020) Printable silver nanowire and PEDOT:PSS nanocomposite ink for flexible transparent conducting applications. ACS Appl Electron Mater 2(4):1000–1010
154. Yuk H, Lu B, Lin S, Qu K, Xu J, Luo J et al (2020) 3D printing of conducting polymers. Nat Commun 11(1):1604
155. Kee S, Haque MA, Corzo D, Alshareef HN, Baran D (2019) Self-healing and stretchable 3D-printed organic thermoelectrics. Adv Func Mater 29(51):1905426
156. Park SH, Su R, Jeong J, Guo SZ, Qiu K, Joung D et al (2018) 3D printed polymer photodetectors. Adv Mater e1803980
157. Hinton TJ, Jallerat Q, Palchesko RN, Park JH, Grodzicki MS, Shue HJ et al (2015) Three-dimensional printing of complex biological structures by freeform reversible embedding of suspended hydrogels. Sci Adv 1(9):e1500758
158. Wang J, Lu T, Yang M, Sun D, Xia Y, Wang T (2019) Hydrogel 3D printing with the capacitor edge effect. Sci Adv 5(3):eaau8769
159. Li H, Tan YJ, Kiran R, Tor SB, Zhou K (2021) Submerged and non-submerged 3D bioprinting approaches for the fabrication of complex structures with the hydrogel pair GelMA and alginate/methylcellulose. Addit Manuf 37:101640
160. Jin Y, Compaan A, Chai W, Huang Y (2017) Functional nanoclay suspension for printing-then-solidification of liquid materials. ACS Appl Mater Interfaces 9(23):20057–20066
161. Zhou L, Ramezani H, Sun M, Xie M, Nie J, Lv S et al (2020) 3D printing of high-strength chitosan hydrogel scaffolds without any organic solvents. Biomater Sci 8(18):5020–5028
162. Yin X-Y, Zhang Y, Cai X, Guo Q, Yang J, Wang ZL (2019) 3D printing of ionic conductors for high-sensitivity wearable sensors. Mater Horiz 6(4):767–780

163. Yin XY, Zhang Y, Xiao J, Moorlag C, Yang J (2019) Monolithic Dual-Material 3D Printing of Ionic Skins with Long-Term Performance Stability. Adv Func Mater 29(39):1904716
164. Wang J, Liu Y, Su S, Wei J, Rahman SE, Ning F et al (2019) Ultrasensitive wearable strain sensors of 3D printing tough and conductive hydrogels. Polymers (Basel). 11(11):1873
165. Zhu Z, Park HS, McAlpine MC (2020) 3D printed deformable sensors. Sci Adv 6(25):eaba5575
166. Gao H, Li J, Zhang F, Liu Y, Leng J (2019) The research status and challenges of shape memory polymer-based flexible electronics. Mater Horiz 6(5):931–944
167. Kuang X, Chen K, Dunn CK, Wu J, Li VCF, Qi HJ (2018) 3D printing of highly stretchable, shape-memory, and self-healing elastomer toward novel 4D printing. ACS Appl Mater Interfaces 10(8):7381–7388
168. Meyers MA, Chen P-Y, Lin AY-M, Seki Y (2008) Biological materials: structure and mechanical properties. Prog Mater Sci 53(1):1–206
169. Abdollahi S, Markvicka EJ, Majidi C, Feinberg AW (2020) 3D printing silicone elastomer for patient-specific wearable pulse oximeter. Adv Healthc Mater 9(15):e1901735
170. Zheng R, Chen Y, Chi H, Qiu H, Xue H, Bai H (2020) 3D printing of a polydimethylsiloxane/polytetrafluoroethylene composite elastomer and its application in a triboelectric nanogenerator. ACS Appl Mater Interfaces 12(51):57441–57449
171. Guo Y, Chen S, Sun L, Yang L, Zhang L, Lou J et al (2020) Degradable and fully recyclable dynamic thermoset elastomer for 3D-printed wearable electronics. Adv Func Mater 31(9):2009799
172. Yao S, Vargas L, Hu X, Zhu Y (2018) A novel finger kinematic tracking method based on skin-like wearable strain sensors. IEEE Sens J 18(7):3010–3015
173. Myers AC, Huang H, Zhu Y (2015) Wearable silver nanowire dry electrodes for electrophysiological sensing. RSC Adv 5(15):11627–11632
174. Chortos A, Liu J, Bao Z (2016) Pursuing prosthetic electronic skin. Nat Mater 15(9):937–950
175. Edwards C, Marks R (1995) Evaluation of biomechanical properties of human skin. Clin Dermatol 13(4):375–380
176. Yao S, Zhu Y (2014) Wearable multifunctional sensors using printed stretchable conductors made of silver nanowires. Nanoscale 6(4):2345–2352
177. Gao Y, Yu G, Shu T, Chen Y, Yang W, Liu Y et al (2019) 3D-printed coaxial fibers for integrated wearable sensor skin. Adv Mater Technol 4(10):1900504
178. Wang Z, Gao W, Zhang Q, Zheng K, Xu J, Xu W et al (2019) 3D-Printed graphene/polydimethylsiloxane composites for stretchable and strain-insensitive temperature sensors. ACS Appl Mater Interfaces 11(1):1344–1352
179. Liu Z, Mo F, Li H, Zhu M, Wang Z, Liang G et al (2018) Advances in flexible and wearable energy-storage textiles. Small Methods 2(11):1800124
180. Praveen S, Santhoshkumar P, Joe YC, Senthil C, Lee CW (2020) 3D-printed architecture of Li-ion batteries and its applications to smart wearable electronic devices. Appl Mater Today 20:100688
181. Magno M, Boyle D (2017) Wearable energy harvesting: from body to battery. In: 2017 12th IEEE international conference on design & technology of integrated systems in Nanoscale Era (Dtis 2017)
182. Khalid S, Raouf I, Khan A, Kim N, Kim HS (2019) A review of human-powered energy harvesting for smart electronics: recent progress and challenges. Int J Prec Eng Manufact-Green Technol 6(4):821–851
183. Zhu M, Zhu F, Schmidt OG (2021) Nano energy for miniaturized systems. Nano Mater Sci 3(2):107–112
184. Zeng W, Tao X-M, Lin S, Lee C, Shi D, Lam K-h, et al. Defect-engineered reduced graphene oxide sheets with high electric conductivity and controlled thermal conductivity for soft and flexible wearable thermoelectric generators. Nano Energy. 2018;54:163–74.
185. Tang Z, Jia S, Shi X, Li B, Zhou C (2019) Coaxial printing of silicone elastomer composite fibers for stretchable and wearable piezoresistive sensors. Polymers (Basel) 11(4):666